

Two-dimensional van der Waals multiferroic tunnel junctions for multi-state, low-power spintronics: A review

Zhi Yan(严志), Jianhua Xiao(肖建华), Ruixia Yang(杨瑞霞), and Xiaohong Xu(许小红)
Citation: Chin. Phys. B, 2026, 35 (**6**): 067304. DOI: 10.1088/1674-1056/ae3c8b
http://cpb.iphy.ac.cn; http://iopscience.iop.org/cpb

What follows is a list of articles you may be interested in

Electron doping in FeSe monolayer and multilayer via metal phthalocyanine adsorption: A first-principles investigation

Fangyu Yang(杨方玉), Yan-Fang Zhang(张艳芳), Peixuan Li(李佩璇), and Shixuan Du(杜世萱)
Chin. Phys. B, 2025, 34 (**11**): 117302. DOI: 10.1088/1674-1056/ae0396

Modulating electronic properties of carbon nanotube via constructing one-dimensional vdW heterostructures

Wenqi Lv(吕雯祺), Weili Li(李伟立), Wei Ji(季威), and Yanning Zhang(张妍宁)
Chin. Phys. B, 2025, 34 (**6**): 067303. DOI: 10.1088/1674-1056/adc406

Bias-induced reconstruction of hybrid interface states in magnetic molecular junctions

Ling-Mei Zhang(张令梅), Yuan-Yuan Miao(苗圆圆), Zhi-Peng Cao(曹智鹏), Shuai Qiu(邱帅), Guang-Ping Zhang(张广平), Jun-Feng Ren(任俊峰), Chuan-Kui Wang(王传奎), and Gui-Chao Hu(胡贵超)
Chin. Phys. B, 2022, 31 (**5**): 057303. DOI: 10.1088/1674-1056/ac3caf

Tunneling magnetoresistance in ferromagnet/organic-ferromagnet/metal junctions

Yan-Qi Li(李彦琪), Hong-Jun Kan(阚洪君), Yuan-Yuan Miao(苗圆圆), Lei Yang(杨磊), Shuai Qiu(邱帅), Guang-Ping Zhang(张广平), Jun-Feng Ren(任俊峰), Chuan-Kui Wang(王传奎), Gui-Chao Hu(胡贵超)
Chin. Phys. B, 2020, 29 (**1**): 017303. DOI: 10.1088/1674-1056/ab5d02

Spin-valley-dependent transport and giant tunneling magnetoresistance in silicene with periodic electromagnetic modulations

Yi-Man Liu(刘一曼), Huai-Hua Shao(邵怀华), Guang-Hui Zhou(周光辉), Hong-Guang Piao(朴红光), Li-Qing Pan(潘礼庆), Min Liu(刘敏)
Chin. Phys. B, 2017, 26 (**12**): 127303. DOI: 10.1088/1674-1056/26/12/127303

TOPICAL REVIEW — Multiferroicity and multicaloric effects

Two-dimensional van der Waals multiferroic tunnel junctions for multi-state, low-power spintronics: A review

Zhi Yan(严志)[1,2], Jianhua Xiao(肖建华)[1], Ruixia Yang(杨瑞霞)[1], and Xiaohong Xu(许小红)[1,2,†]

[1] *School of Materials Science and Engineering & Key Laboratory of Magnetic Molecules and Magnetic Information Materials of Ministry of Education, Shanxi Normal University, Taiyuan* 030031, *China*

[2] *Research Institute of Materials Science & Shanxi Key Laboratory of Advanced Magnetic Materials and Devices Shanxi Normal University, Taiyuan* 030031, *China*

(Received 14 November 2025; revised manuscript received 10 January 2026; accepted manuscript online 23 January 2026)

The convergence of spintronics and multiferroics has enabled unprecedented control of charge and spin degrees of freedom, opening new avenues for multifunctional tunnel junctions. This review provides a systematic overview of multiferroic materials and their integration into tunnel junction devices. First, we categorize multiferroics into type-I, type-II, and heterostructures, discussing synthesis strategies, material design, and approaches for tuning ferroic properties and magnetoelectric coupling. Next, we examine tunnel junctions, including magnetic and ferroelectric types, and focus on multiferroic tunnel junctions (MFTJs), highlighting the mechanisms underlying tunneling magnetoresistance (TMR) and tunneling electroresistance (TER), as well as the roles of interfacial engineering, electrode asymmetry, and multifield control. Special attention is given to emerging two-dimensional van der Waals MFTJs, which offer multi-level data storage, ultralow-power operation, and efficient spin filtering. Finally, we discuss challenges and future directions, emphasizing the importance of room-temperature, strongly coupled 2D multiferroics, scalable fabrication, and interface optimization for next-generation nonvolatile memory and multifunctional spintronic applications.

Keywords: multiferroic tunnel junctions, multiferroic materials, tunneling magnetoresistance, tunneling electroresistance

PACS: 73.40.–c, 75.47.–m, 75.85.+t, 85.75.–d

DOI: 10.1088/1674-1056/ae3c8b **CSTR:** 32038.14.CPB.ae3c8b

1. Introduction

The rapid development of artificial intelligence and Internet of things technologies has imposed increasing demands on information devices with higher storage density, greater functional diversity, and further miniaturization.[1–4] In this context, multiferroic tunnel junctions (MFTJs) have emerged as a new class of multifunctional devices that simultaneously exploit ferroelectric and magnetic order parameters, enabling multistate control through either electric or magnetic fields.[5–7] By coupling the tunneling magnetoresistance (TMR) and tunneling electroresistance (TER) effects within a single junction, MFTJs can achieve multi-resistive nonvolatile memory states, low-power operation, and in-memory computing functionalities. These features offer synergistic control capabilities that surpass those of conventional junctions based on a single ferroic degree of freedom.[8–15]

Conventional three-dimensional (3D) bulk-based MFTJs, however, face significant challenges for practical device integration. At the nanoscale, interfacial defects, lattice mismatch, and surface state pinning can strongly degrade tunneling uniformity, reduce device stability, and limit reproducibility. In addition, bulk materials often exhibit weak magnetoelectric coupling and require complex fabrication processes, including high-temperature epitaxy or layer-by-layer deposition, which are difficult to scale for industrial applications.[16–22] Furthermore, their poor compatibility with silicon-based technologies complicates integration into existing electronic platforms. These intrinsic limitations not only constrain device performance but also motivate the search for alternative material systems that can provide stronger coupling, atomically sharp interfaces, and improved scalability, laying the groundwork for next-generation multifunctional devices.

Two-dimensional (2D) van der Waals (vdW) materials provide a promising solution. Since the isolation of graphene in 2004,[23] a growing variety of 2D vdW systems, such as In_2Se_3,[29] and $MnBi_2Te_4$[30] have been discovered. Their weak interlayer vdW interactions allow the formation of atomically sharp, dangling-bond-free interfaces, effectively reducing interfacial disorder, leakage currents, and scattering effects. In 2D vdW MFTJs, these structural advantages enable simultaneous electric control of magnetism and magnetic control of ferroelectric polarization, supporting versatile operational modes such as electric-write/magnetic-read and magnetic-write/electric-read. Such functionalities provide a solid foundation for in-memory computing, neuromorphic ar-

†Corresponding author. E-mail: xuxh@sxnu.edu.cn

© 2026 Chinese Physical Society and IOP Publishing Ltd. All rights, including for text and data mining, AI training, and similar technologies, are reserved.

chitectures, and multi-state spintronic devices.[31–36] In this review, we systematically summarize recent advances in material systems, magnetoelectric coupling mechanisms, and device functionalities, with an emphasis on emerging 2D vdW MFTJs and their potential applications, as illustrated in Fig. 1. Finally, we provide an outlook on the remaining challenges and future directions in 2D vdW MFTJs, including the discovery of room-temperature, strongly coupled multiferroics; interface engineering; and scalable device integration for next-generation low-power, multifunctional spintronic applications.

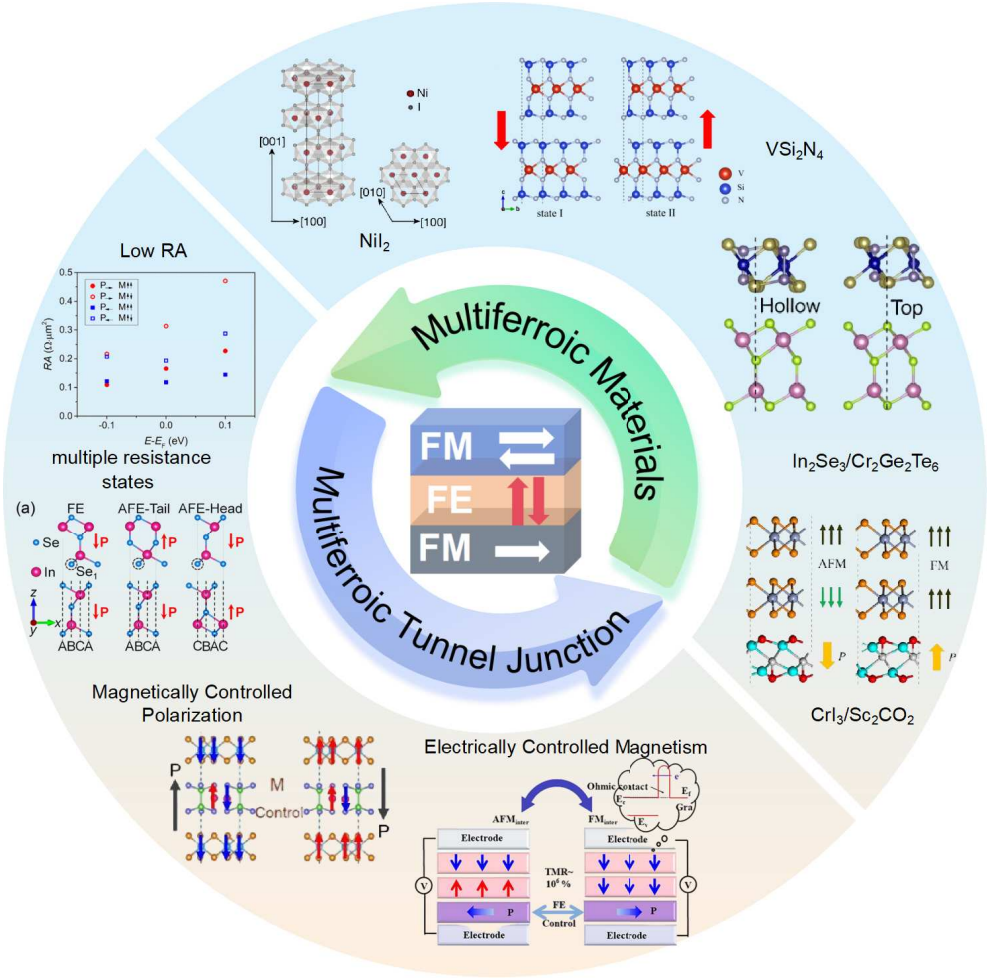


Fig. 1. Schematic overview of two-dimensional van der Waals multiferroic materials and multiferroic tunnel junctions. Reprinted with permission from Refs. [64,92,109,157,159,168–171]. Copyright ©2020 by American Chemical Society. Copyright ©2021 by American Chemical Society. Copyright ©2022 by American Physical Society. Copyright ©2022 by Springer Nature. Copyright ©2023 by American Chemical Society. Copyright ©2024 by American Physical Society. Copyright ©2025 by American Chemical Society.

2. Multiferroic materials

The concept of multiferroic materials was formally introduced by Hans Schmid in 1994, referring to functional materials that simultaneously exhibit two or more ferroic order parameters — such as ferroelectricity, ferromagnetism, ferroelasticity, or ferrotoroidicity — with possible coupling interactions among them.[37,38] A schematic illustration of the four primary ferroic orders and their characteristic hysteresis loops is presented in Fig. 2(a). Among these, the magnetoelectric (ME) coupling effect — the change in electric polarization induced by a magnetic field or the modulation of magnetization by an electric field — has been the most extensively studied. Materials exhibiting strong ME coupling enable electric-field control of magnetism, multistate data storage, and novel sensing functionalities, establishing multiferroics as a central topic at the intersection of condensed matter physics and materials science.[7,39] A major breakthrough occurred in 2003, when Ramesh and co-workers fabricated $BiFeO_3$ (BFO) thin films showing significantly enhanced multiferroic properties compared with bulk crystals [Fig. 3(a)]. In the same year, Tokura and Kimura independently discovered spin-order-induced ferroelectricity in $TbMnO_3$,[40,41] with its structural schematic provided in Fig. 3(b). These advances initiated a period of rapid development in multiferroic research, transitioning the field from fundamental property exploration to functional device realization. However, since around 2016, research activity has gradually slowed, largely due to the practical challenges associated with three-dimensional multiferroics, including limited ME coupling strength and integration

incompatibility with modern device architectures.

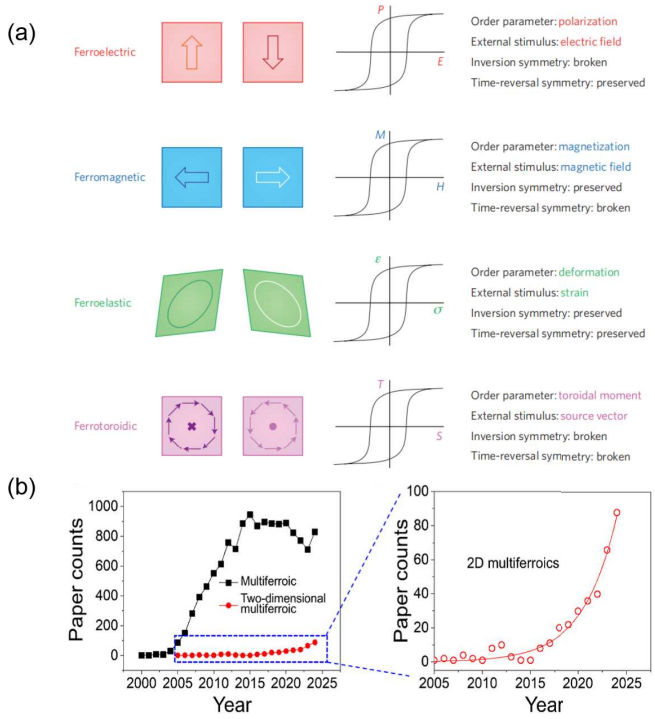


Fig. 2. (a) Schematic illustration of four primary ferroic orders with their corresponding hysteresis loops. Reprinted with permission from Ref. [38]. Copyright ©2012 by Springer Nature. Note: Ferroelasticity is associated with a lowering of point-group symmetry and does not necessarily require inversion-symmetry breaking; depending on the specific ferroelastic transition, inversion symmetry may be preserved or broken. (b) Exponential growth in research on 2D multiferroic materials over recent years. Reprinted with permission from Ref. [42]. Copyright ©2025 by American Chemical Society.

Recently, the emergence of 2D vdW crystals has revitalized this field by providing an atomically thin platform for exploring coupled ferroic orders.[42] As illustrated in Fig. 2(b), the number of publications on 2D multiferroic materials has increased exponentially over the past few years. Despite their technological potential, intrinsic single-phase multiferroics combining ferroelectricity and magnetism remain scarce, primarily due to several fundamental physical constraints.[43] First, symmetry considerations impose strict requirements: ferromagnetism requires the breaking of time-reversal symmetry, while ferroelectricity demands the absence of spatial inversion symmetry. The coexistence of both orders thus necessitates the simultaneous violation of these two symmetries. Second, the microscopic origins of magnetism and ferroelectricity are inherently different. Magnetism typically arises from the spin moments of unpaired d- or f-electrons, which establish long-range order via direct, superexchange, or double-exchange interactions. In contrast, ferroelectricity results from various mechanisms that often compete with magnetic ordering. Based on their microscopic origins and coupling mechanisms, multiferroics can be broadly divided into two categories, as discussed below.

2.1. Type-I multiferroics

Type-I multiferroics feature ferroelectric and magnetic orders that originate from largely independent microscopic mechanisms. These materials typically possess high ferroelectric Curie temperatures (often above room temperature) but relatively weak ME coupling, which limits their technological applicability.[44] Representative examples include bismuth-based perovskite oxides and hexagonal manganites. Among them, BFO is the most prominent example. It crystallizes in a rhombohedral perovskite structure (space group $R3c$), exhibiting a ferroelectric Curie temperature of ~ 1100 K and an antiferromagnetic Néel temperature of ~ 640 K. The large polarization originates from off-center displacements of Bi^{3+} ions driven by their stereochemically active $6s^2$ lone pairs, while Fe^{3+} spins form a G-type antiferromagnetic order. Because the net macroscopic magnetization is weak, approaches such as chemical substitution (e.g., La, Mn) and strain engineering are often employed to enhance its ME response.[45–48] Another important family is the hexagonal $RMnO_3$ system (R = Y, Ho, Lu, Yb; space group $P6_3cm$). In these materials, ferroelectricity arises from asymmetric displacement of Mn^{3+} ions and associated lattice distortions, yielding Curie temperatures between 600 K and 900 K. The Mn^{3+} ions order antiferromagnetically via superexchange interactions, with Néel temperatures around 70–120 K.[49] Compounds such as $YMnO_3$ and $HoMnO_3$ thus exhibit coexisting ferroelectric and antiferromagnetic orders at low temperature.[50–53]

Type-I multiferroics provide a broad class of materials with robust ferroelectricity and thermal stability, yet their weak coupling between ferroic orders limits their use in electric-field-controlled magnetism and spintronic applications.

2.2. Type-II multiferroics

Type-II multiferroics are distinguished by the fact that their ferroelectricity is magnetically induced, i.e., the electric polarization emerges as a direct consequence of a particular magnetic ordering.[54,55] Consequently, ferroelectric and magnetic transitions typically occur within similar temperature ranges and exhibit strong ME coupling. However, both transition temperatures are generally below room temperature, which limits device applications. Representative examples include orthorhombic $DyMnO_3$, trigonal $CuFeO_2$, and monoclinic $MnWO_4$.[56–58] In these materials, non-collinear spin structures, such as spin spirals, break spatial inversion symmetry through the Dzyaloshinskii–Moriya (DM) interaction, while the emergence of electric polarization arises from the combined effects of mechanisms like the inverse DM mechanism and spin-dependent p–d hybridization.[59,60]

The search for intrinsically multiferroic layered materials suitable for nanoelectronic devices has drawn exten-

sive attention. Among these, NiI_2 has recently emerged as a compelling 2D type-II multiferroic.[61,62] These materials exhibit macroscopic polarization in their bulk phases due to the presence of helical magnetic order [Fig. 3(c)]. However, the polarization behavior at the monolayer/bilayer limit remains controversial, and the minimum thickness required to induce finite polarization via helical magnetic order has yet to be determined.[63,64] Furthermore, although $MnPS_3$ exhibits broken inversion symmetry below its Néel temperature,[65] its magnetoelectric coupling has not been directly measured. In contrast, $CuCrP_2S_6$, as a van der Waals layered antiferromagnet,[66] demonstrates spin-induced ferroelectricity and significant magnetoelectric coupling, with substantial polarization retained even at the monolayer limit. More importantly, the polarization in $CuCrP_2S_6$ originates from localized noncentrosymmetric Cr^{3+} sites and is not constrained by helical or noncollinear magnetic order. This provides a more universal material platform for achieving stable type-II multiferroicity in ultrathin dimensions.

Type-II multiferroics demonstrate inherently strong coupling between magnetic and ferroelectric orders, but their low ordering temperatures remain a major obstacle for room-temperature operation.

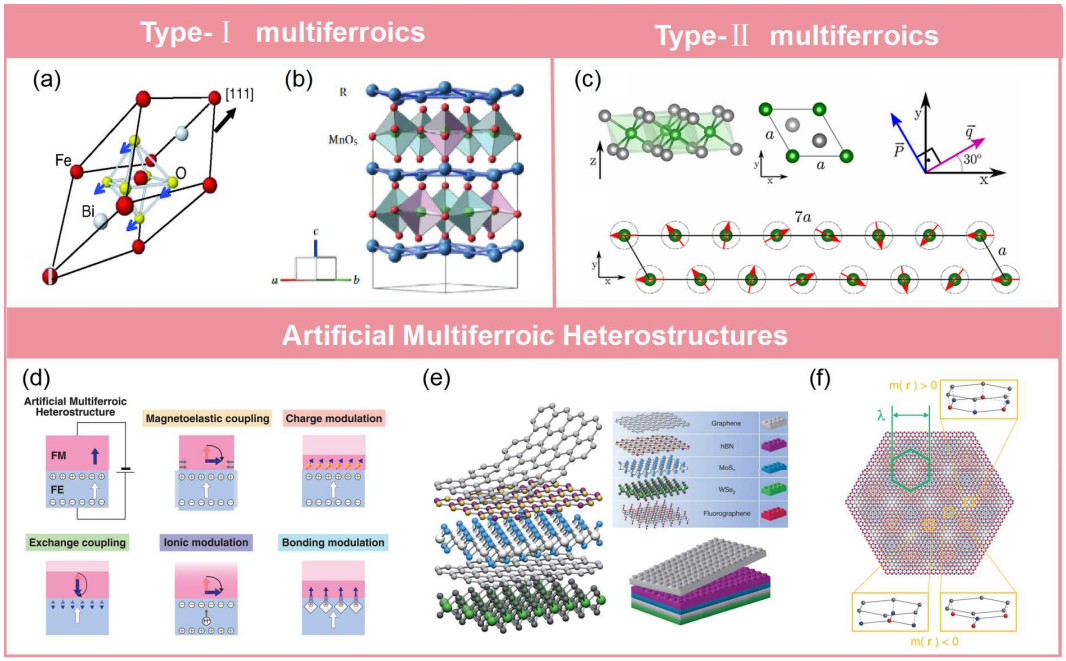


Fig. 3. (a) Unit cell schematic of $BiFeO_3$. Reprinted with permission from Ref. [40]. Copyright ©2003 by the American Association for the Advancement of Science (b) Crystal structure of hexagonal rare-earth manganites with chemical formula $RMnO_3$.[49] (c) Structure of monolayer NiI_2 with nickel and iodine atoms shown in green and gray, respectively. The real-space spin spiral propagation vector (pink) and induced ferroelectric polarization (blue) are indicated. The magnetic spiral order exhibits a 7×1 supercell periodicity.[62] (d) Schematic of a multiferroic heterostructure illustrating the underlying magnetoelectric coupling mechanisms.[68] (e) Architecture of a van der Waals heterostructure. Reprinted with permission from Ref. [83]. Copyright ©2013 by Springer Nature. (f) Moiré pattern formed in graphene/boron nitride heterostacks. Reprinted with permission from Ref. [96]. Copyright ©2013 by the American Association for the Advancement of Science.

3. Multiferroic heterostructure

Compared with intrinsic single-phase materials, artificial multiferroic heterostructures composed of ferroelectric and ferromagnetic layers provide greater flexibility in material choice and interfacial design.[67–70] These systems exhibit enhanced magnetoelectric coupling and host novel physical phenomena and control mechanisms, as illustrated in Fig. 3(d). Rather than relying on intrinsic multiferroicity, these heterostructures achieve electric control of magnetism or magnetic control of polarization through atomic-scale interfacial coupling. Key mechanisms include strain transfer, charge reconstruction, orbital hybridization, and exchange bias, enabled by external fields. This approach provides a versatile pathway toward next-generation high-performance devices such as high-density memories, magnetoelectric sensors, spintronic components, and microwave systems.[71–77] Representative three-dimensional bulk multiferroic heterostructures include $CoFe/BaTiO_3$,[78] $BiFeO_3/CoFe$,[79] $La_{0.7}Sr_{0.3}MnO_3$/PMN-PT,[80,81] and $EuTiO_3$/Ca-$SrTiO_3$.[82]

With the ongoing evolution of 2D materials research, the focus of multiferroic heterostructure studies has shifted from conventional bulk architectures toward vdW heterostructures.[83–87] As illustrated in Fig. 3(e), these systems can be assembled using a "materials LEGO" approach, where atomically thin layers with distinct properties are stacked via weak vdW interactions. This strategy enables precise interfacial engineering of multiple ferroic orders and their couplings. The emergence of 2D fer-

romagnets (e.g., CrI_3, Fe_3GeTe_2) and ferroelectrics (e.g., α-In_2Se_3) around 2016 provided essential building blocks for such architectures.[29,88–91] The emergence of these materials provided the fundamental building blocks for multiferroic heterostructures, prompting theoretical investigations into the possibility of stacking them via van der Waals integration. Early studies predicted possible magnetoelectric coupling effects at the interface. Since 2017, extensive theoretical work based on first-principles calculations has systematically revealed electric-field control of magnetic anisotropy, interlayer magnetic coupling, and electronic phase transitions in systems such as $In_2Se_3/Cr_2Ge_2Te_6$,[92] In_2Se_3/CrI_3,[93] Sc_2CO_2/VSe_2,[94] and $MnCl_3/CuInP_2S_6$.[95] More recently, twisted moiré superlattices have been proposed to further enrich magnetoelectric phenomena by tuning interlayer interactions at the nanoscale,[96–99] as shown in Fig. 3(f).

Artificial multiferroic heterostructures, especially vdW-based ones, combine structural precision with functional tunability, offering a powerful platform for achieving controllable ME coupling and device integration.

3.1. Property engineering and magnetoelectric control

The development of intrinsic multiferroics that operate at or above room temperature remains limited by the scarcity of suitable material systems and their generally weak magnetoelectric (ME) coupling, which hampers practical applications. Consequently, property manipulation has become a central strategy in multiferroics research, aiming to enhance ME coupling strength, increase ferroic ordering temperatures, and minimize energy consumption. Key approaches include chemical composition design, external-field modulation, and interface or strain engineering.[100–102] Chemical composition engineering through elemental doping represents a widely adopted strategy for tuning crystal structures and electronic properties via atomic substitution. In the prototypical multiferroic BFO, doping with rare-earth elements (e.g., Er, La, Nd, Sm) or transition metals (e.g., Mn, Cr) effectively suppresses oxygen vacancy formation and modulates lattice distortions, thereby enhancing both ferroelectric polarization and magnetic performance. Figure 4(a) presents XRD patterns of rare-earth-doped BFO.[103–106] Alternatively, anion doping (such as fluorine incorporation) can modify electronic structure and carrier concentration, further regulating spin ordering and polarization behavior. As shown in Fig. 4(b), F-doped BFO exhibits significantly increased remnant polarization.[107]

Electric field control stands out among external-field modulation strategies for its ability to nonvolatilely manipulate magnetic anisotropy and magnetization in adjacent ferromagnetic layers by switching the polarization of ferroelectric components. This mechanism is of considerable importance in multiferroic heterostructures. In the van der Waals heterostructure $In_2Se_3/Cr_2Ge_2Te_6$, for instance, upward polarization of In_2Se_3 induces in-plane magnetic anisotropy in $Cr_2Ge_2Te_6$, while downward polarization switches the easy axis to out-of-plane, enabling direct electric-field control of magnetic behavior. Figure 4(c) presents the orbital-projected band structures of $In_2Se_3/Cr_2Ge_2Te_6$ under different polarization states.[92] In some cases, ferroelectric polarization switching can even drive electronic phase transitions. For example, in the Sc_2CO_2/CrI_3 heterostructure, CrI_3 maintains its intrinsic semiconducting behavior when the Sc_2CO_2 layer is polarized upward, but downward polarization drives the spin-up conduction band across the Fermi level, converting the system into a half-metallic state,[108] as shown in Fig. 4(d). Furthermore, electric-field-induced polarization switching in Sc_2CO_2 can reversibly tune the interlayer magnetic coupling in bilayer CrI_3 between ferromagnetic and antiferromagnetic configurations [Fig. 4(e)],[109] effectively switching magnetism "on" and "off". A similar mechanism has been observed in the $GdClBr/CuBiP_2Se_6$ van der Waals multiferroic heterostructure: during the reversal of ferroelectric polarization in $CuBiP_2Se_6$, the ferromagnetic GdClBr monolayer undergoes a transition from a semiconductor to a half-metal. Further research has revealed the synergistic regulatory effect of strain on the interface of this system: under strain, the amount of charge transfer at the $GdClBr/CuBiP_2Se_6$ heterojunction interface increases with increasing strain, while the Curie temperature of the system decreases with increasing strain. More importantly, the perpendicular (out-of-plane) magnetic anisotropy significantly enhances with increasing compressive strain. This finding indicates that ferroelectric polarization and strain can synergistically influence magnetic coupling strength and magnetic ordering temperature by modulating interface charge transfer and electronic structure, offering a new pathway for realizing multifunctional electrically controlled magnetic devices.[110,111]

Advances in synthesis and property manipulation have significantly expanded the design space of multiferroics, enabling atomic-level control over structure–property relationships and paving the way for scalable integration of multiferroic functionalities into practical device architectures. The studies reviewed above establish a comprehensive understanding of the structural design, physical mechanisms, and controllability of multiferroic materials — from bulk perovskites to 2D vdW heterostructures. These advances not only deepen our insight into magnetoelectric coupling but also provide the material foundation for tunnel junction devices, where coupled ferroic orders govern electron transport. In the following section, we focus on tunnel junctions, including magnetic tunnel junctions, ferroelectric tunnel junctions, and multiferroic tunnel junctions, to elucidate how multiferroicity can be harnessed to achieve nonvolatile, multistate, and low-power information functionalities.

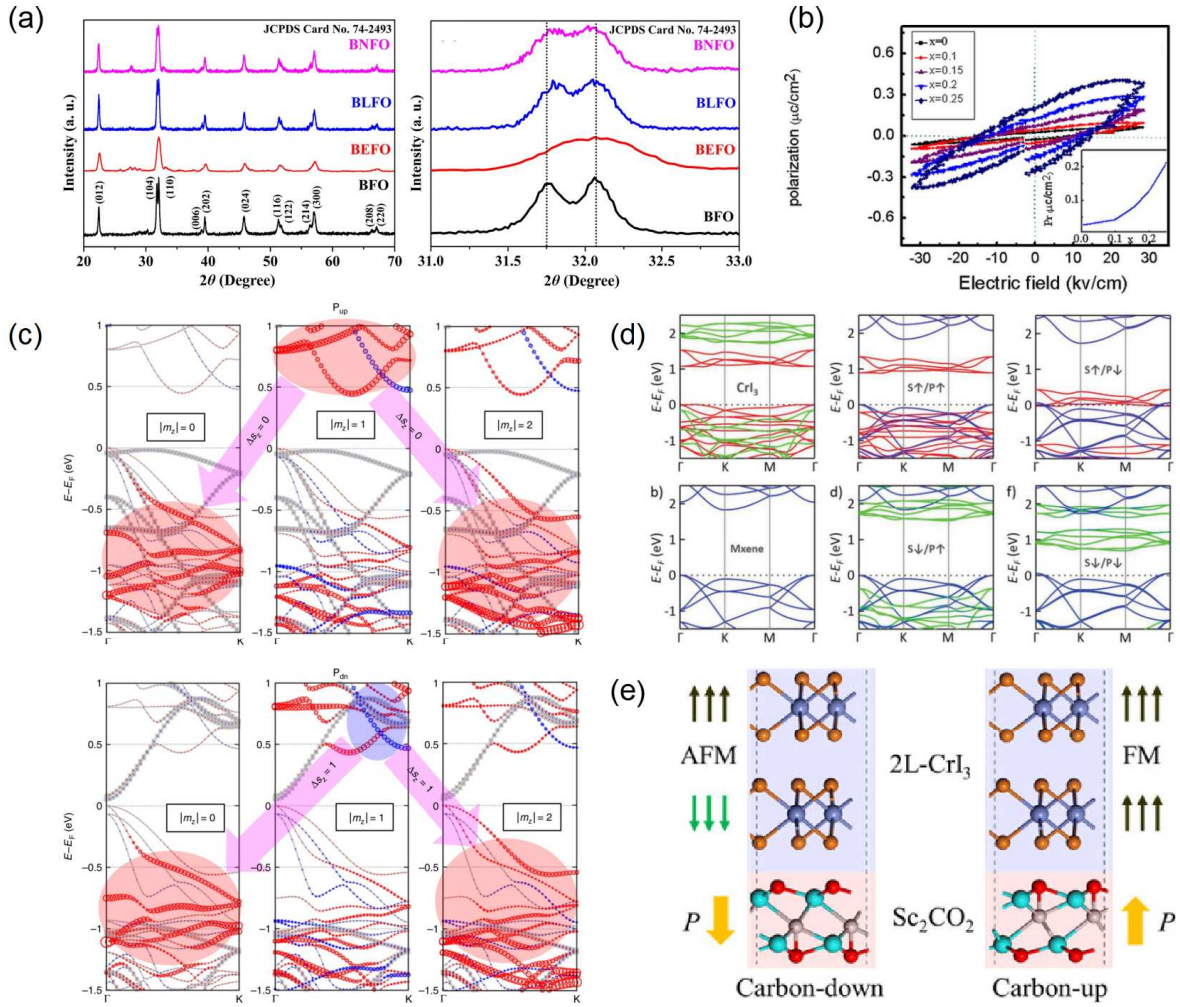


Fig. 4. (a) XRD patterns of BFO, $Bi_{0.95}Er_{0.05}FeO_3$, $Bi_{0.95}La_{0.05}FeO_3$, and $Bi_{0.95}Nd_{0.05}FeO_3$ samples (left), with magnified view between 31°–33° (right). Reprinted with permission from Ref. [106]. Copyright ©2020 by the Minerals, Metals & Materials Society. (b) PE hysteresis loops of FBFO, showing remnant polarization (P_r) increasing from ~ 0.0253 μC·cm^{-2} ($x = 0$) to ~ 0.2118 μC·cm^{-2} ($x = 0.25$). Reprinted with permission from Ref. [107]. Copyright ©2024 by the Minerals, Metals & Materials Society. (c) Orbital-projected band structures of $Cr_2Ge_2Te_6/In_2Se_3$ heterostructure under different polarization states: upward (top) and downward (bottom). Red and blue circles denote majority- and minority-spin states, respectively.[92] (d) Electronic band structures of CrI_3, MXene (Sc_2CO_2), CrI_3/P↑-Sc_2CO_2, and CrI_3/P↓-Sc_2CO_2 heterostructures. Red and green lines represent spin-up (S↑) and spin-down (S↓) contributions from CrI_3, while blue lines indicate Sc_2CO_2 contributions. Reprinted with permission from Ref. [108]. ©2019 by WILEY–VCH Verlag GmbH & Co. KGaA, Weinheim. (e) Bilayer CrI_3/Sc_2CO_2 heterostructure. Thin black and green arrows denote spin orientations in bilayer CrI_3; thick gold arrows indicate out-of-plane polarization direction in Sc_2CO_2. Reprinted with permission from Ref. [109]. Copyright ©2020 by American Chemical Society.

4. Tunnel junctions

Tunnel junctions represent a fundamental class of quantum devices characterized by a sandwich-like architecture consisting of two electrodes separated by a thin insulating barrier, through which electrons can tunnel quantum mechanically.[112,113] The field originated from mid-20th-century theoretical and experimental studies of quantum tunneling. Landmark discoveries in the 1960s by Giaever and Esaki demonstrated electron tunneling across different barrier systems, while Josephson predicted coherent tunneling between superconductors. Their seminal contributions, recognized by the 1973 Nobel Prize in Physics, established the conceptual foundation of modern tunneling devices.[114–116] Subsequent decades witnessed rapid advances in MTJs, particularly following the observation of room-temperature tunneling magnetoresistance (TMR) in the 1990s. A major breakthrough came in 2004 with the implementation of crystalline MgO barriers, which dramatically enhanced TMR ratios and propelled spintronic devices toward practical applications.[117–119] Recent progress in thin-film epitaxy and 2D material synthesis has further diversified junction architectures. FTJs exploit polarization reversal in ferroelectric barriers to produce tunneling electroresistance (TER), while MFTJs integrate ferroelectric and magnetic orders — either within single-phase multiferroics or artificially engineered heterostructures — to achieve magnetoelectric-coupled functionality.[120–123]

4.1. Magnetic tunnel junctions and ferroelectric tunnel junctions

Before examining MFTJs in detail, it is instructive to trace the development of their structural and functional precur-

sors — MTJs and FTJs — which provide critical insights into spin-dependent transport and ferroelectric tunneling phenomena. MTJs, as the more technologically mature system, have enabled efficient manipulation of spin-polarized transport and laid the industrial foundation for non-volatile spintronic memory. The extensive experience gained in interface engineering, barrier optimization, and device integration of MTJs has provided valuable guidance for advancing FTJs and, by extension, MFTJs.[124,125]

The concept of the MTJ was first proposed by Julliere in 1975. Its canonical structure consists of a magnetic metal electrode/insulating barrier/magnetic metal electrode.[126] In such a system, one electrode acts as a reference layer with fixed magnetization, while the other serves as a free layer whose magnetization can be switched by an external magnetic field, generating a TMR effect. The TMR ratio — defined as the relative change in resistance between parallel and antiparallel magnetization configurations — is a central figure of merit for MTJ performance and depends sensitively on both the electrode spin polarization and the barrier electronic properties. Owing to limitations in thin-film growth technologies, research progressed slowly for two decades following Julliere's proposal.[127,128] In 1995, Miyazaki *et al.* achieved a room-temperature TMR of 18% in Fe/Al_2O_3/Fe junctions, revitalizing global interest in MTJs.[129–132] Continuous improvements in material quality and epitaxial precision have since elevated room-temperature TMR values to over 600% by 2023,[133] as illustrated in Fig. 5(a). The emergence of 2D magnets has injected new vitality into MTJ research. Yan *et al.* systematically investigated the electronic transport properties of Cu/CrI_3/BN/*n*-CrI_3/Cu (n = 1, 2, 3, 4) MTJs using density-functional theory. Their calculations showed that for $n = 3$, the junction yields fully spin-polarized currents under equilibrium, with a TMR ratio approaching 3600%,[134] as depicted in Fig. 5(b). However, the low Curie temperature of CrI_3 restricts its practical viability. Identifying intrinsic 2D magnetic materials with higher Curie or Néel temperatures is therefore essential for room-temperature MTJ operation.[135–137] Metallic or half-metallic systems such as Fe_3GeTe_2 and $Mn_2Ge_2Te_6$, exhibiting Curie temperatures above 200 K, have emerged as promising candidates,[138–140] as illustrated in Figs. 5(c) and 5(d). These materials can serve as spin-polarized electrodes in van der Waals (vdW) MTJs, providing lower interface resistance and higher TMR ratios compared to insulating barriers like CrI_3.

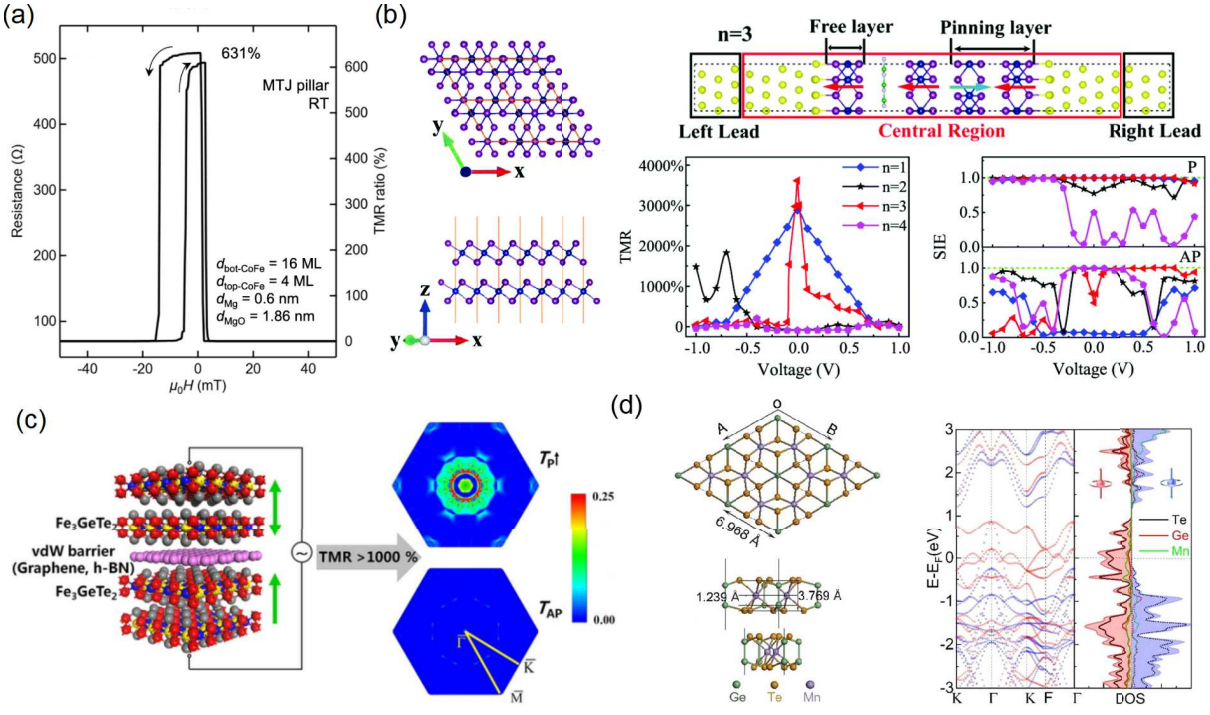


Fig. 5. (a) Highest reported room-temperature TMR in MgO-barrier magnetic tunnel junctions.[133] (b) Top and side views of CrI_3 (left); tunnel junction model of Cu/CrI_3/BN/3CrI_3/Cu and corresponding TMR vs. bias voltage under parallel (P) and antiparallel (AP) configurations (right). Reprinted with permission from Ref. [134]. Copyright ©2020 by Royal Society of Chemistry. (c) Magnetic tunnel junction model of Fe_3GeTe_2/h-BN/Fe_3GeTe_2 (left); electron tunneling probability across the 2D Brillouin zone (right). Reprinted with permission from Ref. [138]. Copyright ©2019 by American Chemical Society. (d) Top and side views of $Mn_2Ge_2Te_6$ (left); spin-polarized band structure and projected density of states (PDOS) (right). Reprinted with permission from Ref. [140]. Copyright ©2022 by American Chemical Society.

The concept of the FTJ was formally introduced by Kohlstedt *et al.* in 2005.[141] An FTJ typically comprises an ultrathin ferroelectric barrier sandwiched between two metallic electrodes. Its operation relies on the TER effect: reversing the ferroelectric polarization direction via an electric field modulates the tunneling potential profile and induces large, re-

versible resistance changes.[142,143] Current research on FTJs has largely focused on perovskite and oxide ferroelectrics. Perovskite-based FTJs offer large TER ratios but suffer from poor compatibility with silicon technology, whereas oxide-based FTJs exhibit better integration potential but generally lower TER.[144–146] Recent advances in 2D ferroelectric materials, such as In_2Se_3, Sc_2CO_2, and MoSeS, have introduced new possibilities for nanoscale, low-power FTJs.[29,147–149]

4.2. Multiferroic tunnel junction

Parallel to the resurgence of multiferroic and magnetoelectric research, FTJ development has evolved into the broader concept of MFTJs. The hallmark of MFTJs is the coexistence of TMR and TER effects, enabling dual-field (electric and magnetic) control and multi-resistance-state operation.[150–152] Schematic representations of different tunnel junction types are shown in Fig. 6(a).

The theoretical foundation of MFTJs was established in 2006, when Duan *et al.* identified interfacial magnetoelectric coupling in $Fe/BaTiO_3$ heterostructures.[153] Subsequent designs, such as $Co/BaTiO_3/Co$ and $Fe/BaTiO_3/Fe$ MFTJs [Fig. 6(b)], demonstrated enhanced coupling when fully spin-polarized ferromagnetic electrodes were employed.[154] In 2009, Velev *et al.* predicted coexisting TMR and TER effects in $SrRuO_3/BaTiO_3/SrRuO_3$ junctions, which were later experimentally verified by Gajek *et al.*,[155,156] as shown in Fig. 6(c). Despite the significant progress achieved with three-dimensional perovskite barriers, these systems face intrinsic limitations in nanoscale integration due to lattice mismatch, interfacial imperfections, and complex fabrication processes.

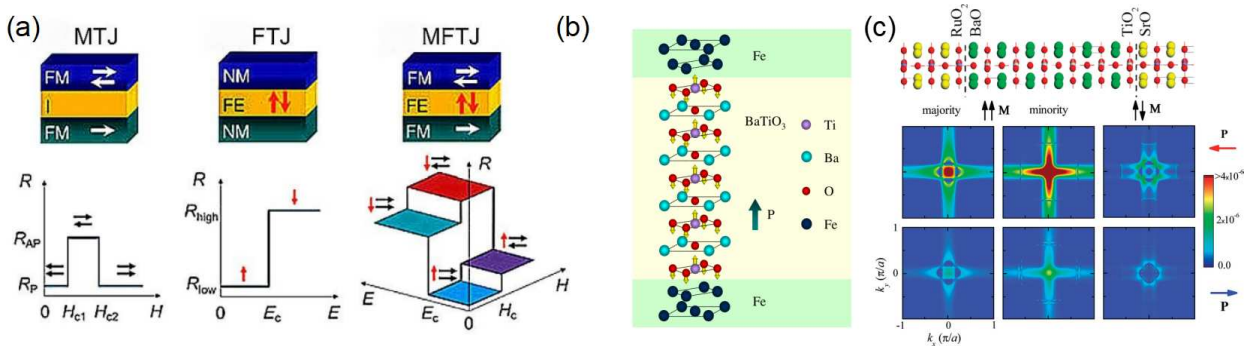


Fig. 6. (a) Schematic diagrams of different tunnel junction types: MTJ, FTJ, and MFTJ. Ferromagnetic, ferroelectric, normal metal, and insulating (I) layers are indicated. The plots below show the resistance response of each junction to magnetic (H) and electric (E) fields. Horizontal and vertical arrows denote the directions of magnetization and ferroelectric polarization, respectively. Reprinted with permission from Ref. [150]. Copyright ©2012 by the Materials Research Society. (b) Structure of the $Fe/BaTiO_3/Fe$ multiferroic tunnel junction. Reprinted with permission from Ref. [153]. Copyright ©2006 by American Physical Society. (c) $SrRuO_3/BaTiO_3/SrRuO_3$ MFTJ and its transmission spectrum in the 2D Brillouin zone. Reprinted with permission from Ref. [155]. Copyright ©2009 by American Chemical Society.

In contrast, 2D vdW materials provide an attractive alternative platform. Their atomically thin nature, lack of dangling bonds, and flexible stacking configurations collectively suppress interface disorder and facilitate strong magnetoelectric coupling across atomically sharp interfaces. First-principles studies have predicted that vdW MFTJs can simultaneously achieve low resistance-area (RA) products and large TMR/TER ratios, making them promising for next-generation high-density, low-power spintronic memories. For instance, Su *et al.*[157] investigated the spin transport properties in $Fe_mGeTe_2/In_2Se_3/Fe_nGeTe_2$ ($m,n = 3, 4, 5$; $m \neq n$) junctions, demonstrating multi-resistance-state control through the coupling of ferroelectric polarization and magnetic order. The calculated RA product is below 1 $\Omega \cdot \mu m^2$, suggesting excellent scalability, as illustrated in Fig. 7(a). Subsequently, an even lower RA ($< 0.1\ \Omega \cdot \mu m^2$) was reported in $CrSe_2/CuInP_2S_6/CrSe_2$ (CS/CIPS/CS) MFTJs,[158] as shown in Fig. 7(b). Nevertheless, current 2D vdW MFTJs still exhibit relatively modest TMR and TER ratios, and the low Curie temperatures of most 2D magnetic materials remain a key bottleneck for room-temperature operation.

To enhance the performance of MFTJs, systematic investigations have been conducted focusing on electrode materials and structural design. On the one hand, exploring two-dimensional magnetic materials with high T_c and high performance has become crucial. Yan *et al.*[159] constructed a six-state nonvolatile MFTJ using Fe_3GeTe_2 electrodes (Curie temperature of 220 K) and a bilayer α-In_2Se_3 ferroelectric barrier. This junction exhibited remarkably large TMR and TER ratios of 1.1×10^7% and 744%, respectively, which could be further enhanced under applied strain, as shown in Fig. 7(c). Even more groundbreaking is that Yu *et al.*[160] reported a ferromagnetic Mn_2Se_3 monolayer with an exceptionally high Curie temperature of 820 K and intrinsic half-metallicity, underscoring its potential for spintronic applications. Building upon this, Sun *et al.*[161] incorporated Mn_2Se_3 as a spin-filtering layer in a Mn_2Se_3/bilayer-In_2Se_3/$TiTe_2$ vdW MFTJ, achieving notable TMR and TER ratios of 6237% and 1771%, respectively, under finite bias. The device exhibited four distinguishable resistance states, demonstrating its suitability for multi-level nonvolatile memory. Moreover, arranging such junctions into an $N \times N$ array can enable in-memory computing archi-

tectures. The crystal structure, electronic band structure of Mn_2Se_3, and the schematic of its multi-level storage mechanism are presented in Fig. 7(d). On the other hand, structural designs such as adjusting the barrier thickness and employing asymmetric electrodes can also significantly enhance device performance. Zhu *et al.*[162] modulated the MnSe barrier thickness ($n = 24$), achieving TMR and TER ratios as high as 1.4×10^6% and 4114%, respectively. The use of asymmetric Cu/Fe_3GeTe_2 electrodes further enhanced the TER ratio. This structure also demonstrated excellent spin-filtering characteristics, indicating its potential for multi-state memory and spin-control device applications. The corresponding device model is illustrated in Fig. 7(e).

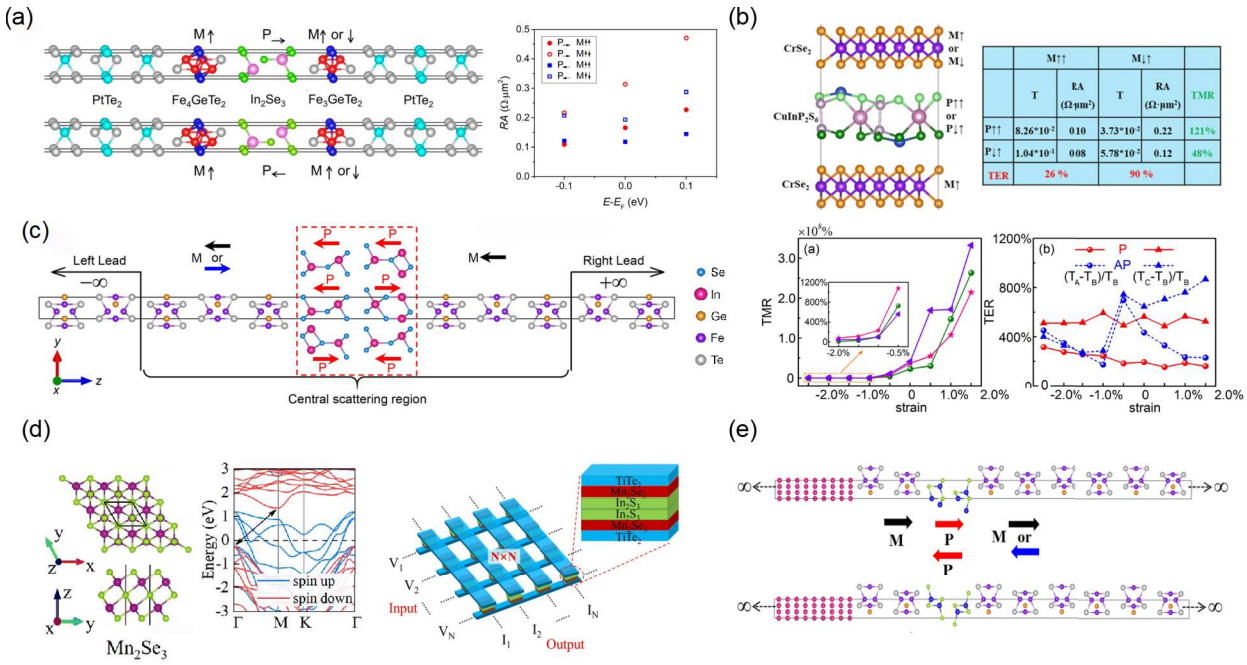


Fig. 7. (a) Atomic structure of the $PtTe_2/Fe_4GeTe_2/\alpha$-$In_2Se_3/Fe_3GeTe_2/PtTe_2$ multiferroic tunnel junction and the corresponding resistance-area (RA) values for multiple resistance states within the Fermi energy range ($E_F \pm 0.1$ eV). Reprinted with permission from Ref. [157]. Copyright ©2021 by American Chemical Society. (b) Structure of the CS/CIPS/CS junction and its RA values under different resistance states. Reprinted with permission from Ref. [158]. Copyright ©2021 by American Chemical Society. (c) Schematic of an FGT/BIS/FGT multiferroic tunnel junction using metallic Fe_3GeTe_2 electrodes with three distinct polarization configurations (left); strain dependence of TMR and TER under various polarization states. Reprinted with permission from Ref. [159]. Copyright ©2022 by American Physical Society. (d) Crystal structure and electronic band structure of Mn_2Se_3 (top), with a schematic of the multi-level storage mechanism using an $N \times N$ MFTJ array (bottom). Reprinted with permission from Ref. [161]. Copyright ©2024 by Royal Society of Chemistry. (e) Device configuration of the Cu/Fe_3GeTe_2/2L-MnSe/Fe_3GeTe_2 heterostructure. Reprinted with permission from Ref. [162]. Copyright ©2024 by Royal Society of Chemistry.

The vdW MFTJs are typically constructed by vertically stacking ferroelectric and ferromagnetic layers. While this architecture enables basic multiferroicity, it inevitably inherits the intrinsic limitations of conventional ferroelectrics, where polarization reversal is driven by ionic displacement and requires overcoming large energy barriers. As a result, such devices often suffer from high power consumption and polarization fatigue. Recently, the concept of sliding ferroelectricity has emerged as a promising solution to these challenges.[163–165] This phenomenon originates from interlayer sliding between adjacent atomic planes, which breaks spatial inversion symmetry and induces an out-of-plane polarization. Since the switching process involves only weak vdW interlayer forces, sliding ferroelectrics exhibit ultralow energy consumption, fast switching kinetics, and non-destructive cycling behavior. This mechanism not only overcomes the high energy barrier inherent to conventional ferroelectrics but also introduces an additional degree of freedom for manipulating magnetoelectric coupling in 2D-confined systems. Experimental demonstrations in hexagonal boron nitride (h-BN) and transition metal dichalcogenides have established sliding ferroelectricity as a transformative route toward next-generation ultralow-power electronic and spintronic devices. Weak interlayer vdW interactions enable vertical sliding ferroelectricity in bilayer h-BN. Dong *et al.*[166] designed an MFTJ using sliding ferroelectric bilayer h-BN as the tunnel barrier. As illustrated in Fig. 8(a), the Coulomb potential along the transport direction (z-axis) exhibits distinct modulations in the central scattering region of the FGT/Gr/h-BN/Gr/CrI_3 junction. First-principles calculations of the transport properties reveal that switching the magnetic configuration from parallel to antiparallel alignment yields a TMR ratio of 3.36×10^4% at a bias of 0.2 V. Furthermore, sliding-induced switching of the h-BN stacking order from AB to BA results in a TER ratio of approximately 6.68×10^3% under the same bias conditions [Fig. 8(b)].

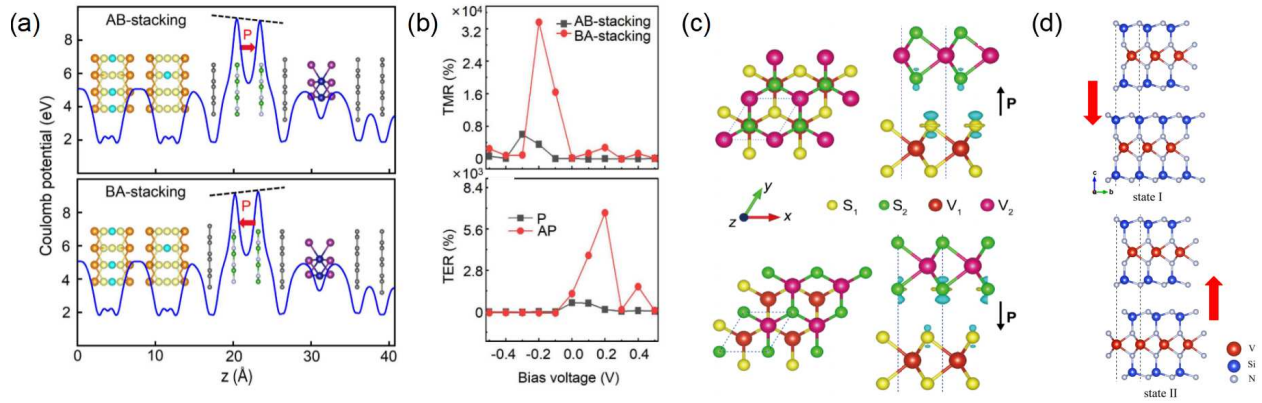


Fig. 8. (a) Evolution of the Coulomb potential along the transport direction (z-axis) in the central scattering region of the FGT/Gr/h-BN/Gr/CrI_3 vdW MFTJ. Reprinted with permission from Ref. [166]. Copyright ©2023 by American Physical Society. (b) TMR and TER ratios as functions of bias voltage in the FGT/Gr/h-BN/Gr/CrI_3 MFTJ. Reprinted with permission from Ref. [166]. Copyright ©2024 by American Physical Society. (c) Schematic of the bilayer VS_2 crystal structure. (d) Schematic of the bilayer VSi_2N_4 crystal structure. Reprinted with permission from Ref. [168]. Copyright ©2024 by American Physical Society.

The functional scope of sliding degrees of freedom has further expanded from single ferroelectricity to multiferroic coupling, giving rise to the concept of sliding multiferroics. Bilayer VS_2 integrates intrinsic multiferroicity, interlayer antiferromagnetism, and sliding ferroelectricity within a single system, making it an ideal platform for vdW intrinsic MFTJs [Fig. 8(c)].[167] Similarly, bilayer VSi_2N_4 exhibits intrinsic multiferroicity, characterized by out-of-plane ferroelectricity coupled with interlayer A-type antiferromagnetism. Ferroelectricity and antiferromagnetism couple via ferrovalley order, enabling electric-field control of magnetism through interlayer sliding [Fig. 8(d)].[168] Although sliding ferroelectricity in multilayer magnetic materials shows great potential, its polarization switching typically relies on external electric fields or mechanical stress to induce atomic migration, which may still introduce additional energy consumption and affect device stability. Therefore, developing homologous monolayer intrinsic multiferroic materials holds promise for achieving efficient and stable magnetoelectric coupling and polarization control at a more fundamental level, representing a key direction for advancing the next generation of van der Waals multiferroic tunnel junctions.[169]

Despite these advances, current vdW MFTJs predominantly rely on mechanically stacked ferroelectric and magnetic layers, which lack intrinsic magnetoelectric coupling. This limitation restricts device performance and elevates power consumption, making the establishment of direct magnetoelectric coupling a critical challenge. Two primary mechanisms have been identified: (i) electric-field-controlled magnetization mediated by ferroelectric polarization, and (ii) magnetic-field-controlled polarization reversal. In 2023, Yu *et al.*[170] reported fully electric-field-controlled operation in a trilayer vdW multiferroic heterostructure comprising CrI_3/$AgBiP_2Se_6$ and $Cr_2Ge_2Te_6$/In_2Se_3 [Figs. 9(a) and 9(b)]. In this architecture, the magnetic state of the bilayer can be reversibly switched by reversing the polarization of the adjacent ferroelectric layers, a phenomenon attributed to polarization-induced band structure modulation and interfacial charge transfer. A graphene-electrode device based on this heterostructure achieved near-ideal Ohmic contact [Fig. 9(c)]. In the complementary direction of magnetic control of ferroelectric polarization, Yan *et al.*[171] demonstrated a fully magnetically controlled vdW MFTJ using a $CrBr_3$/$MnPSe_3$/$CrBr_3$ heterostructure, where polarization reversal occurs without inversion-symmetry-breaking atomic migration [Fig. 9(d)]. First-principles spin-polarized transport calculations indicate that asymmetric $PtTe_2$/alkali-metal-doped/intercalated $CrBr_3$ electrodes yield exceptional performance, with a TMR ratio of 3.6×10^7% and a TER ratio of 9990% over a broad bias range. Remarkably, the device exhibits a pronounced negative differential resistance effect, with a peak-to-valley ratio of 9.55×10^9% — the highest reported value in vertical tunnel junctions [Figs. 9(e)–9(g)].

Conventional vdW MFTJs with the configurations of normal metal/ferromagnet/ferroelectric face several challenges, including susceptibility to external stray magnetic fields and interfacial coupling issues. In recent years, antiferromagnetic materials have gained attention due to their ultrafast spin dynamics, negligible stray fields, robustness against external perturbations, and terahertz-frequency dynamic characteristics.[172–175] Compared to ferromagnetic systems, antiferromagnetic devices offer faster operation speeds. Integrating 2D vdW antiferromagnets with ferroelectric materials in tunnel junctions thus provides a promising platform for antiferromagnetic MFTJs. For example, Yan *et al.* designed an antiferromagnetic/ferroelectric barrier/antiferromagnetic heterostructure using bilayer $MnBi_2Te_4$/In_2Se_3/bilayer $MnBi_2Te_4$ as a prototype. By tuning both the magnetization configurations of the multilayer $MnBi_2Te_4$ and the polarization orientation of the In_2Se_3 barrier, up to 16 distinct nonvolatile resistance states can be accessed and controlled, as illustrated in

Fig. 10(a). The predicted maximum TMR and TER values are $3.79 \times 10^4\%$ and $2.41 \times 10^5\%$, respectively, under equilibrium conditions.[176] Recent experimental advances further highlight the potential of antiferromagnetic multiferroic materials. In 2024, $CuCrSe_2$ was demonstrated to exhibit both ferroelectric and ferromagnetic order at room temperature, establishing it as an ideal candidate for vdW MFTJs.[177] Building on this, He *et al.*[178] proposed a fully bilayer $CuCrSe_2$-based vdW MFTJ, wherein the material intrinsically adopts an A-type antiferromagnetic and antiferroelectric ground state. Polarization switching from the antiferroelectric to ferroelectric state concurrently induces a transition from antiferromagnetic to ferromagnetic order within a single unit, thereby enabling simultaneous control of spin and ferroelectric polarization. Figure 10(b) compares the TER, TMR, and RA performance of the graphene/bilayer $CuCrSe_2$/graphene junction with representative 2D material tunnel junctions at zero bias. These results underscore the significant potential of antiferromagnetic MFTJs for high-performance, low-power spintronic applications.

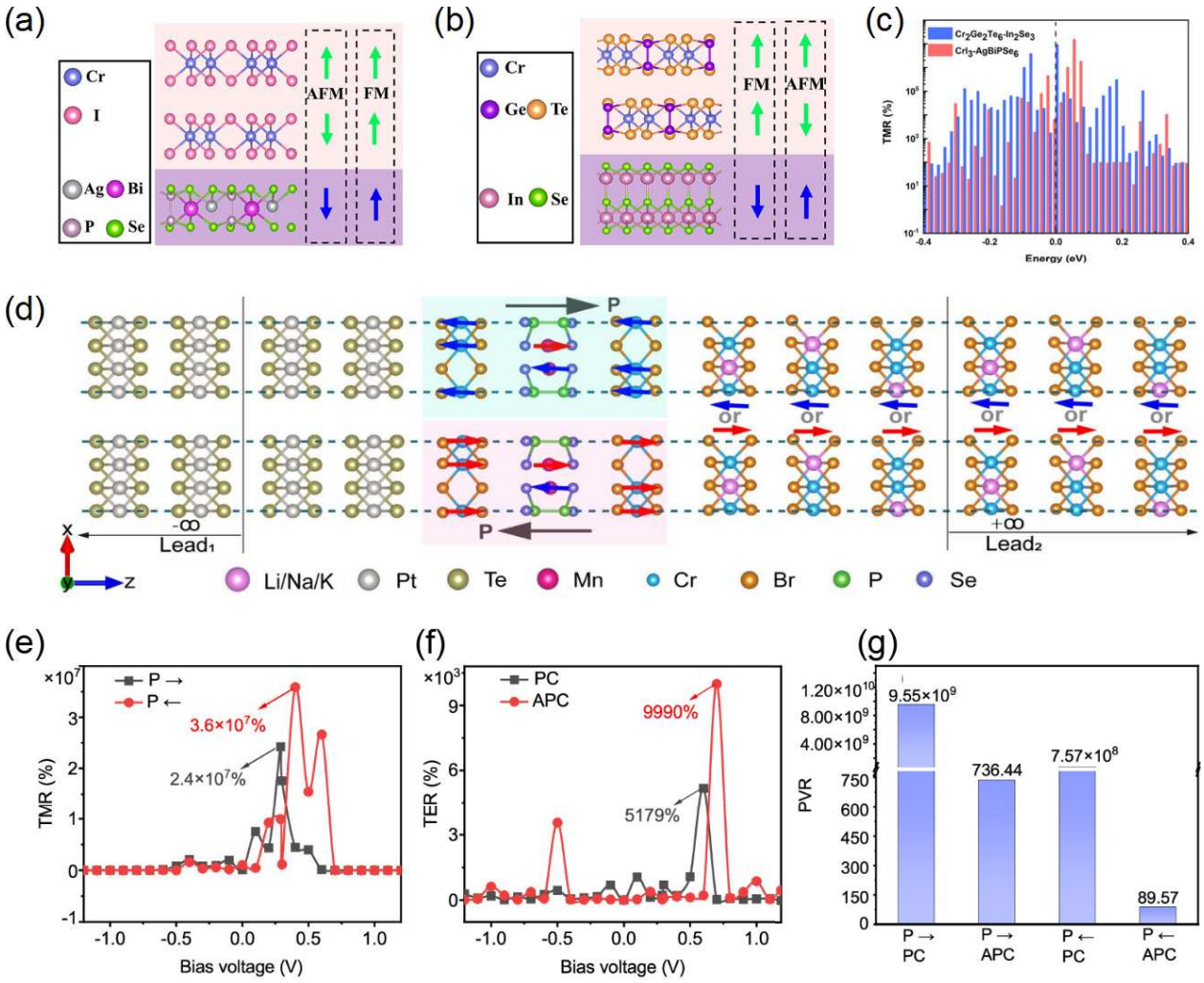


Fig. 9. (a) $CrI_3/AgBiP_2Se_6$ heterostructure. (b) $Cr_2Ge_2Te_6/In_2Se_3$ heterostructure. Green arrows indicate spin alignment in the magnetic bilayer, while blue arrows denote the direction of ferroelectric polarization. (c) TMR ratios for the two distinct heterostructures: $CrI_3/AgBiP_2Se_6$ and $Cr_2Ge_2Te_6/In_2Se_3$. Reprinted with permission from Ref. [170]. Copyright ©2023 by American Chemical Society. (d) Schematic of the $PtTe_2/CrBr_3/MnPSe_3/CrBr_3/CrBr_3$(Li/Na/K) vdW MFTJ device model. (e) TMR ratio in $PtTe_2/CrBr_3/MnPSe_3/CrBr_3/CrBr_3$(Li) MFTJs under different polarization directions and magnetic configurations. (f) TER ratio. (g) Current peak-to-valley ratio (PVR). Reprinted with permission from Ref. [171]. Copyright ©2025 by American Chemical Society.

To advance antiferromagnetic spintronics, there is a pressing need for highly sensitive and reliable electrical methods to detect the Néel vector. In non-collinear antiferromagnets, spin-split Fermi surfaces can generate spin-polarized currents that are tunable via external driving currents and modulated by the relative orientation of the Néel vectors in two antiferromagnetic electrodes.[179,180] This mechanism provides a novel electrical detection strategy for antiferromagnetic spintronics, with implications for both fundamental studies and device applications. Notably, the Néel vector in non-collinear antiferromagnets can rotate continuously in 3D space without vanishing, a unique property that enables high-density memory and magnetoelectric functionality.[181,182] Mn_3Sn, a prototypical non-collinear antiferromagnet with geometrically frus-

trated magnetic moments, exhibits Weyl semimetallic behavior alongside coexisting ferromagnetic- and ferroelectric-like orders at room temperature. Its crystal structure and electronic band structure are shown in Figs. 10(c) and 10(d).[183,184] Mn_3Sn displays pronounced spintronic features, including momentum-dependent spin splitting and the anomalous Hall effect, with electrically switchable spin states. Its robust thermal stability and electronic properties make it an attractive candidate for MFTJs and spintronic devices.[185,186] For example, He *et al.* investigated spin-dependent transport in an Mn_3Sn/BN/α-In_2Se_3/Mn_3Sn MFTJ. The junction resistance can be tuned by controlling both the Néel vector orientation in Mn_3Sn and the polarization direction in α-In_2Se_3, enabling multiple nonvolatile resistance states, as illustrated in Fig. 10(e). Theoretical predictions indicate a TMR ratio up to 6650% and a TER ratio exceeding 8000%.[187] Comparable spin-split band structures and TMR effects have been predicted in other non-collinear antiferromagnetic metals, including Mn_3Ge, Mn_3Ga, Mn_3Pt, and Mn_3GaN.[188–192]

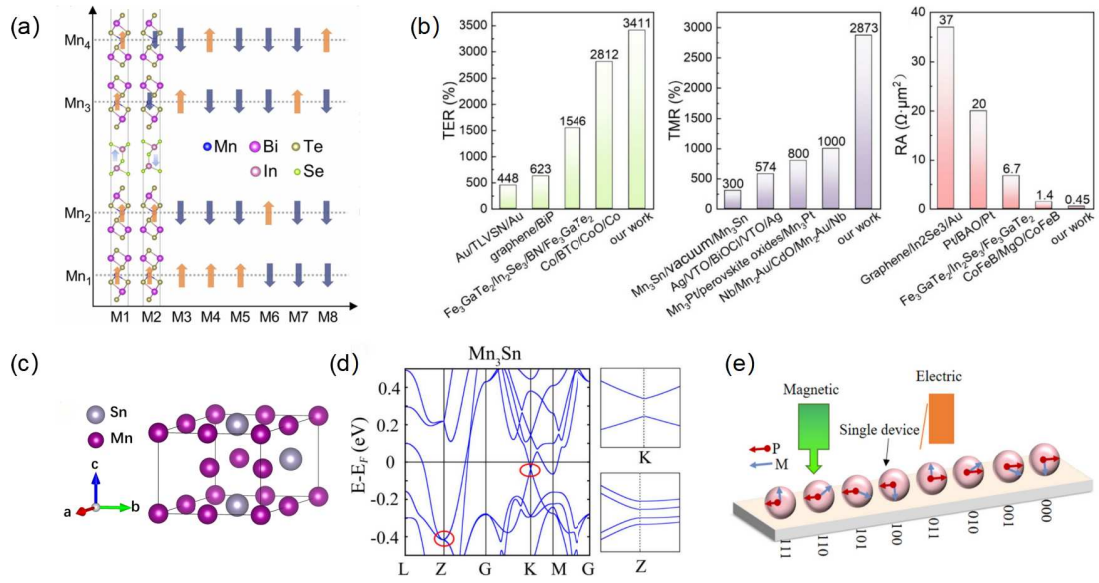


Fig. 10. (a) Magnetic configuration of Mn atoms in the MBT-2L/IS/MBT-2L structure. Reprinted with permission from Ref. [176]. Copyright ©2025 by American Physical Society. (b) Performance comparison at zero bias: TER ratio, TMR ratio, and RA product of the graphene/bilayer $CuCrSe_2$/graphene structure versus recently reported 2D material tunnel junctions. Reprinted with permission from Ref. [178]. Copyright ©2025 by American Chemical Society. (c) Crystal structure of Mn_3Sn. Reprinted with permission from Ref. [184]. Copyright ©2025 by American Chemical Society. (d) Band structure of Mn_3Sn with spin–orbit coupling included; insets show magnified views near the *Z* and *K* points (highlighted by red circles).[183] (e) Schematic of operational resistance states for multi-level data storage in an MFTJ. Blue arrows indicate the relative orientation of the Néel vectors in the left and right electrodes; red arrows denote polarization directions. Eight distinct resistance states can be achieved by tuning magnetic and electric fields, enabling three-bit storage. Reprinted with permission from Ref. [187]. Copyright ©2024 American Physical Society.

Very recently, altermagnets — collinear magnetic materials with fully compensated moments but non-relativistic momentum-dependent spin splitting — have emerged as a new class of spintronic materials. Unlike conventional ferromagnets, antiferromagnets, or ferrimagnets, altermagnets exhibit substantial spin polarization in momentum space while maintaining zero macroscopic magnetization. This combination confers multiple advantages, including low power consumption, high non-volatility, ultrafast spin dynamics, and immunity to stray fields, making them promising for high-density magnetic memory and miniaturized spin-logic devices.[193–197] Typical examples include CrSb, MnTe, MnF_2, and V_2Te_2O, which offer versatile platforms for exploring novel spin control mechanisms and developing next-generation spintronic architectures.[198–200] For altermagnet-based MTJs, theoretical studies predict that structures such as Ag/V_2Te_2O/BiOCl/V_2Te_2O/Ag can achieve a TMR of 574%, although spin-filtering remains limited.[201] However, room-temperature MTJs with altermagnets and tunable TMR or multiferroically modulated TER remain largely unexplored. Recently, Zhang *et al.*[202] designed a room-temperature MFTJ based on a CrSb/In_2Se_3/Fe_3GaTe_2 heterostructure, integrating an altermagnet, a ferroelectric barrier, and a ferromagnetic electrode. This junction exhibits a TMR of 2308%, a TER of 707%, and nearly perfect spin-filtering efficiency. All constituent materials possess high critical temperatures, good lattice matching, and feasible synthesis routes, making them suitable for high-performance MFTJs. While 3D CrSb demonstrates excellent properties, the development of 2D altermagnets with similar characteristics could further overcome current structural constraints.

Overall, research on MFTJs has progressed from fundamental exploration toward function-oriented design. By integrating emerging material systems, including 2D materials, antiferromagnetic orders, and altermagnets, MFTJs are increasingly surpassing the limits of conventional magneto-

electric control. They exhibit remarkable potential for multistate memory, ultra-low-power computation, and adaptive sensing. Looking forward, precise heterointerface engineering and cross-scale property control may establish MFTJs as key components in post-Moore information technologies, advancing spintronics toward quantum-enabled and intelligent device architectures.

4.3. Experimental advances in vdw multiferroic heterostructures for multiferroic tunnel junctions

Indeed, theoretical studies on two-dimensional van der Waals multiferroic tunnel junctions have outlined an exciting blueprint, predicting enormous tunneling magnetoresistance and electroresistance effects.[203,204] However, the maturation of an emerging field relies not only on theoretical guidance but also on experimental validation and engineering solidification. Although complete van der Waals multiferroic tunnel junctions that operate stably at room temperature with excellent performance remain in the exploratory stage, significant progress has been made in the field: experimental research on van der Waals heterostructures based on two-dimensional magnetic and ferroelectric materials has achieved substantial breakthroughs.

These advancements, while not yet directly manifesting as fully realized "sandwich"-style tunnel junction devices, have systematically addressed their core constituent units. Two-dimensional single-phase multiferroic materials, with their intrinsic magnetoelectric coupling effects, offer an ideal physical platform for exploring novel quantum phenomena and achieving efficient electric-field control of magnetism. Theoretically predicted monolayer $Hf_2VC_2F_2$ is a type-II multiferroic with a relatively high phase transition temperature, whose ferroelectric polarization is directly induced by a unique 120° Y-type antiferromagnetic structure, exhibiting magnetically controlled electrical properties; however, achieving the reverse, electrically controlled magnetism, remains challenging.[205] Similarly, the sliding ferroelectricity observed in bilayer VS_2, while offering a novel ultra-low-energy polarization switching mechanism, suffers from environmental instability at the atomically thin scale, limiting its potential for device integration.[206] More instructively, in CrOCl, researchers have successfully demonstrated the feasibility of multi-resistance-state storage based on multiferroic order by achieving ultra-high-density, ultra-low-energy continuous information storage in micrometer-scale devices through the cooperative control of magnetic and electric fields.[207] However, these single-phase materials, including the recently prominent NiI_2 and $CuCrP_2S_6$, all face an unavoidable common bottleneck: their magnetic ordering temperatures are far below room temperature, fundamentally constraining their prospects for practical applications.

To overcome the inherent performance and temperature limitations of single-phase materials, the research paradigm has shifted toward van der Waals multiferroic heterostructures, which offer greater engineering flexibility. By stacking high-performance two-dimensional ferroelectrics with emerging two-dimensional magnetic materials on demand, robust magnetoelectric coupling can be "engineered" at the artificial interface. This strategy not only circumvents the typical trade-off in single-phase materials between high operating temperature and strong coupling but also enables more efficient and stable electric-field control of magnetism through the synergy of multiple coupling mechanisms such as band alignment and strain. This paves a practical new pathway for developing multiferroic tunnel junctions and spintronic devices for room-temperature applications.

Recent experimental studies have fully demonstrated the immense potential of van der Waals multiferroic heterostructures for electric-field control of magnetism. Liang *et al.*, using a $Cr_2Ge_2Te_6$/ferroelectric polymer P(VDF-TrFE) heterostructure at 4 K, achieved non-volatile magnetic modulation, observing synchronous changes in coercivity and remanent magnetization, highlighting the central role of interfacial coupling.[208] At 80 K, Eom *et al.* demonstrated voltage-controlled magnetism in an $Fe_{3-x}GeTe_2/\alpha$–In_2Se_3 heterostructure, attributing the mechanism to in-plane strain transfer through combined Raman spectroscopy and first-principles calculations.[209] Similarly, at a low temperature of 10 K, Wu *et al.* utilized ferroelectric polarization in a CrI_3/α-In_2Se_3 system to achieve a non-volatile modulation of up to 82% in the critical magnetic switching field with a gate voltage of only 5 V.[210] While these works successfully validated the feasibility of electric-field magnetic control, the poor environmental stability and extremely low operating temperatures underscore the urgency of exploring van der Waals multiferroic systems capable of stable operation at room temperature.

Encouragingly, this challenge is being overcome. Using a simple bonding method to construct an Fe_5GeTe_2/ferroelectric substrate PMN-PT multiferroic heterostructure, strong electric-field control of magnetization has been achieved at room temperature for the first time via strain-mediated magnetoelectric coupling. The unique butterfly-shaped magnetoelectric hysteresis loop not only confirms effective interfacial coupling but also enables non-volatile bistable memory, representing significant progress in the design of energy-efficient spintronic devices.[211] Following this trend, the van der Waals ferromagnet Fe_3GaTe_2 (Curie temperature of 350–380 K) and ferroelectric $CuInP_2S_6$ (Curie temperature of $\sim$ 315 K) have emerged as an ideal combination due to their outstanding intrinsic room-temperature properties. The $Fe_3GaTe_2/CuInP_2S_6$ multiferroic heterostructure, successfully fabricated by Zhao *et al.*, demonstrated robust, non-volatile electrical control of

magnetism at room temperature for the first time.[212] This work marks a critical step for the field, transitioning from a low-temperature proof-of-concept to a room-temperature functional demonstration, thereby laying a solid material and experimental foundation for developing practical, low-power magnetoelectric memory and logic devices based on van der Waals multiferroic heterostructures.

Controlled synthesis is fundamental to realizing magnetoelectric coupling and functional device performance. Current approaches for fabricating multiferroic materials primarily include physical vapor deposition (PVD), chemical vapor deposition (CVD), and mechanical exfoliation.[213–215] In 2022, Song *et al.* achieved controlled growth of bulk and few-layer NiI_2 by PVD using NiI_2 powder as the precursor and hexagonal boron nitride as a substrate, benefiting from its atomically flat surface, chemical inertness, and thermal stability,[62] as shown in Fig. 11(a). Although intrinsic 2D multiferroics provide ideal single-phase platforms for ME coupling, their material diversity is still limited. To overcome this, researchers have fabricated vdW multiferroic heterostructures by artificially stacking functional 2D layers.[83,87,216] Two main fabrication strategies are employed: (i) Mechanical exfoliation and dry transfer, in which thin flakes are isolated using elastomers (e.g., PDMS) and then aligned under optical microscopy to construct hybrid stacks. This method provides high design flexibility but low throughput,[209,217] as illustrated in Figs. 11(b) and 11(c). (ii) CVD growth, where vapor-phase precursors react on substrates to directly form 2D materials, enabling wafer-scale heterostructures. Figure 11(d) shows a schematic of a CVD-grown 1T-$CrTe_2$ single crystal. Although scalable, this approach still faces challenges in achieving atomically uniform interfaces.[218–220]

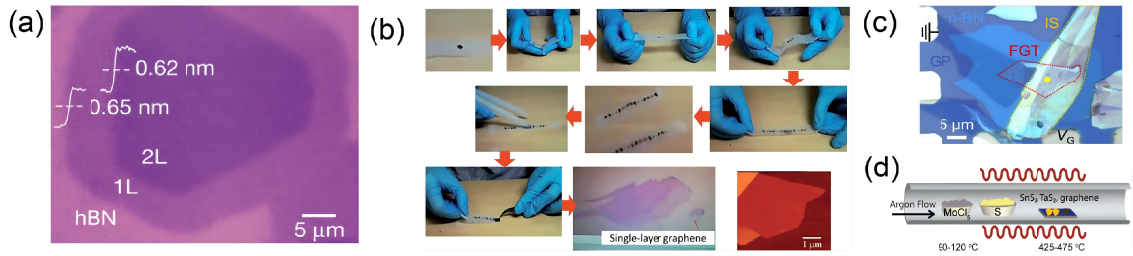


Fig. 11. (a) Optical image of monolayer (1L) and bilayer (2L) NiI_2 samples grown on h-BN via physical vapor deposition. Reprinted with permission from Ref. [62]. Copyright ©2022 by Springer Nature. (b) Mechanical exfoliation process. Reprinted with permission from Ref. [217]. Copyright ©2015 by Royal Society of Chemistry. (c) Optical micrograph of an FGT/IS heterostructure device.[209] (d) Schematic of a CVD grown 1T-$CrTe_2$ single crystal. Reprinted with permission from Ref. [219]. Copyright ©2016 by American Chemical Society.

The current wealth of experimental work on heterostructures essentially involves conducting indispensable "unit testing" and "proof-of-concept" for eventual multiferroic tunnel junctions. These studies address fundamental questions: Does coupling exist? Is it sufficiently strong? These achievements lay a solid physical foundation and provide valuable process expertise for subsequently integrating the complete device structure of a "magnetic electrode–ferroelectric barrier–magnetic electrode." Future breakthroughs will depend on building upon existing heterostructure research to tackle more complex integration challenges, such as electrode contact engineering, the uniformity of ultrathin barriers, and elevating the operating temperature to room temperature. Experimental exploration is steadily progressing from validating coupling principles to a new stage of constructing functional devices.

5. Conclusion and perspectives

The 2D van der Waals multiferroic tunnel junctions (vdW MFTJs) have emerged as a promising platform for multifunctional spintronic devices at the intersection of condensed matter physics and materials science. By combining 2D ferromagnetic, ferroelectric, and multiferroic constituents, vdW MFTJs enable nonvolatile resistance switching via quantum tunneling, with multiple resistance states accessible through electric-field-controlled polarization, magnetic-field-tuned magnetic order, and other stimuli such as strain, offering a route toward high-density memory and adaptive electronics. Concurrently, the materials landscape has expanded from conventional hetero-stacked systems to intrinsic multiferroics, non-collinear antiferromagnets, and altermagnets, enriching the accessible physical attributes and device functionalities. On the theory side, first-principles-based transport studies, often combining density-functional theory with nonequilibrium Green's function methods, have established a framework for understanding the underlying mechanisms and have clarified the roles of electrode spin polarization, ferroelectric tunability, interfacial coupling, and electrode asymmetry in determining device performance. Despite these advances, major challenges persist: many 2D magnets exhibit low Curie temperatures, strongly coupled multiferroics operating at room temperature remain scarce, the diversity of intrinsic 2D multiferroics is still limited and scalable synthesis is difficult, and device-level issues such as contact resistance and interfacial scattering can compromise reproducibility.

Looking ahead, 2D vdW MFTJs provide a flexible platform for exploring multi-state resistance control and spin-

dependent transport in low-dimensional systems. Although practical applications will require continued advances in material synthesis and device engineering, promising material platforms — such as sliding ferroelectric/antiferromagnetic hybrids, Janus monolayers, and moiré systems — are expected to offer viable routes toward room-temperature, strongly coupled 2D vdW multiferroics. These developments could enable robust device functionalities beyond conventional memory, including neuromorphic sensing and logic-in-memory.

Moreover, several fundamental questions that are directly device-relevant remain open, including how robust ferroelectric polarization is stabilized in angstrom-thick tunnel barriers under metallic screening and depolarization fields, and how atomic-scale registry/twist-induced reconstruction reshapes band alignment and exchange proximity, thereby governing the variability and scalability of TER/TMR.

To transition from theoretical predictions to prototype devices, several experimental milestones need to be addressed: (i) high-quality, large-area synthesis of 2D multiferroic building blocks, particularly sliding ferroelectric/antiferromagnetic systems and Janus monolayers; (ii) interface engineering — combining electrostatic screening control (e.g., electrode asymmetry or vdW spacers) with deterministic registry/twist control — to stabilize polarization in angstrom-thick barriers and to reproducibly tune band alignment and exchange proximity; (iii) mitigating contact resistance and interfacial scattering to improve device stability and reproducibility; and (iv) achieving room-temperature operation with strongly coupled multiferroic functionality. By addressing these challenges, 2D vdW MFTJs are poised to play an important role in spintronics, memory technologies, and neuromorphic computing, paving the way toward practical, low-power multifunctional devices.

Acknowledgments

Project supported by the National Natural Science Foundation of China Regional Innovation and Development Joint Fund Key Program (Grant No. U24A6002), the National Natural Science Foundation of China (Grant No. 12304148), and the Shanxi Natural Science Basic Research Program (Grant No. 202203021222219).

References

[1] Wolf S A, Awschalom D D, Buhrman R A, Daughton J M, von Molnár V S, Roukes M L, Chtchelkanova A Y and Treger D M 2001 *Science* **294** 1488
[2] Krishnan K M, Pakhomov A B, Bao Y, Blomqvist P, Chun Y, Gonzales M, Griffin K and Roberts B K 2006 *J. Mater. Sci.* **41** 793
[3] Žutić I, Fabian J and Sarma S D 2004 *Rev. Mod. Phys.* **76** 323
[4] Gu L, Gu X, Zhu X and Sun X 2019 *Adv. Mater.* **31** 1805355
[5] Pantel D, Goetze S, Hesse D and Alexe M 2012 *Nat. Mater.* **11** 289
[6] Yin Y and Li Q 2017 *J. Materiomics* **3** 245
[7] Zhang Y, Li X, Sheng J, Yu S, Zhang J and Su Y 2023 *Appl. Phys. Lett.* **123** 192402
[8] Yin Y W, Raju M, Hu W J, Burton J D, Kim Y M, Borisevich A Y, Pennycook S J, Yang S Y, Noh T W, Gruverman A, Li X G, Zhang Z D, Tsymbal E Y and Li Q 2015 *J. Appl. Phys.* **117** 172601
[9] Gruverman A, Wu D, Lu H, Wang Y, Jang H W, Folkman C M, Zhuravlev M Y, Felker D, Rzchowski M, Eom C B and Tsymbal E Y 2009 *Nano Lett.* **9** 3539
[10] Peng S Z, Zhang Y, Wang M X, Zhang Y G and Zhao W 2014 *Wiley Encyclopedia of Electrical and Electronics Engineering*
[11] Yang W, Xu Y, Li S, Han J, Lin X and Zhao W 2025 *Sci. China Mater.* **68** 1622
[12] Wang X, Zhu C, Deng Y, Duan R, Chen J, Zeng Q, Zhou J, Fu Q, You L, Liu S, Edgar J H, Yu P and Liu Z 2021 *Nat. Commun.* **12** 1109
[13] Yu X, Zhang X, Ma L and Wang J 2024 *Adv. Funct. Mater.* **34** 2409281
[14] Yang F, Tang M H, Ye Z, Zhou Y C, Zheng X J, Tang J X, Zhang J J and He J 2007 *J. Appl. Phys.* **102** 044504
[15] Guo X H, Zhang J, Yao K L and Zhu L 2025 *Adv. Funct. Mater.* **35** 2423855
[16] Hu W and Yang J 2017 *J. Mater. Chem. C* **5** 12289
[17] Duong D L, Yun S J and Lee Y H 2017 *ACS Nano* **11** 11803
[18] Burch K S, Mandrus D and Park J G 2018 *Nature* **563** 47
[19] Zhang Y, Xu H, Feng J, Wu H, Yu G and Han X 2021 *Chin. Phys. B* **30** 118504
[20] Sun Y, Niu G, Ren W, Meng X, Zhao J, Luo W, Ye Z and Xie Y H 2021 *ACS Nano* **15** 10982
[21] Lin Y C, Torsi R, Younas R, Hinkle C L, Rigosi A F, Hill H M, Zhang K, Huang S, Shuck C E, Chen C, Lin Y, Maldonado-Lopez D, Maldonado-Cortes J L, Ferrier J, Kar S, Nayir N, Rajabpour S, Duin A C T, Liu X, Jariwala D, Jiang J, Shi J, Mortelmans W, Jaramillo R, Lopes J M J, Engel-Herbret R, Trofe A, Ignatova T, Lee S H, Mao Z, Damian L, Wang Y, Steves M A, Jr K L K, Wang Z, Law S, Bepete G, Zhou D, Lin J, Scheurer M S, Li J, Wang P, Yu G, Wu S, Akinwande D, Redwing J M and Terrones Robinson J A 2023 *ACS Nano* **17** 9694
[22] Dai M, Wang Z, Wang F, Qiu Y, Zhang J, Xu C Y, Zhai T, Cao W, Fu Y, Jia D, Zhou Y and Hu P A 2019 *Nano Lett.* **19** 5410
[23] Novoselov K S, Geim A K, Morozov S V, Jiang D E, Zhang Y, Dubonos S V, Grigorieva I V and Firsov A A 2004 *Science* **306** 666
[24] Shirodkar S N and Waghmare U V 2014 *Phys. Rev. Lett.* **112** 157601
[25] Manzeli S, Ovchinnikov D, Pasquier D, Yazyev O V and Kis A 2017 *Nat. Rev. Mater.* **2** 1
[26] Wickramaratne D, Weston L and Van de Walle C G 2018 *J. Phys. Chem. C* **122** 25524
[27] Wang H, Huang X, Lin J, Cui J, Chen Y, Zhu C, Liu F, Zeng Q, Zhou J, Yu P, Wang X, He H, Tsang S H, Gao W, Suenge K, Ma F, Yang C, Lu L, Yu T, Teo E H T, Liu G and Liu Z 2017 *Nat. Commun.* **8** 394
[28] Zhang K, Han S, Lee Y, Coak M J, Kim J, Hwang I, Son S, Shin J, Lim M, Jo D, Kim D, Lee H W and Park J G 2021 *Adv. Mater.* **33** 2004110
[29] Ding W, Zhu J, Wang Z, Gao Y, Xiao D, Gu Y, Zhang Z and Zhu W 2017 *Nat. Commun.* **8** 14956
[30] An Y, Wang K, Gong S, Hou Y, Ma C, Zhu M, Zhao C, Wang T, Ma S, Wang H, Wu R and Liu W 2021 *npj Comput. Mater.* **7** 45
[31] Lottermoser T, Lonkai T, Amann U, Hohlwein D, Ihringer J and Fiebig M 2004 *Nature* **430** 541
[32] Hur N, Park S, Sharma P A, Ahn J S, Guha S and Cheong S W 2004 *Nature* **429** 392
[33] Chiba D, Fukami S, Shimamura K, Ishiwata N, Kobayashi K and Ono T 2011 *Nat. Mater.* **10** 853
[34] Matsukura F, Tokura Y and Ohno H 2015 *Nat. Nanotechnol.* **10** 209
[35] Huang B, Clark G, Klein D R, MacNeill D, Navarro-Moratalla E, Seyler K L, Wilson N, McGuire M A, Cobden D H, Xiao D, Yao W, Jarillo-Herrero P and Xu X 2018 *Nat. Nanotechnol.* **13** 544
[36] Zhang W, Gao B, Tan J, Yao P, Yu S, Chang M F, Yoo H J, Qian H and Wu H 2020 *Nat. Electron.* **37** 371
[37] Schmid H 1994 *Ferroelectrics* **162** 317
[38] Bibes M 2012 *Nat. Mater.* **11** 354
[39] Yang J, Wu B, Zhou J, Lu J, Yang J and Shen L 2023 *Nanoscale* **15** 16103
[40] Wang J B N J, Neaton J B, Zheng H, Nagarajan V, Ogale S B, Liu B, Vaithyanathan V, Schlom D G, Waghmare U V, Spaldin N A, Rabe K M, Wuttig M and Ramesh R 2003 *Science* **299** 1719

[41] Kimura T, Goto T, Shintani H, Ishizaka K, Arima T H and Tokura Y 2003 *Nature* **426** 55
[42] Tang Z, Hu Y, Rogée L, Liu D and Lau S P 2025 *Chem. Mater.* **37** 4925
[43] Hill N A 2000 *J. Phys. Chem. B* **104** 6694
[44] Khomskii D I 2006 *J. Magn. Magn. Mater.* **306** 1
[45] Pradhan A K, Zhang K, Hunter D, Dadson J B, Loiutts G B, Bhattacharya P, Katiyar R, Zhang J, Sellmyer D J, Roy U N, Cui Y and Burger A 2005 *J. Appl. Phys.* **97** 093903
[46] Catalan G and Scott J F 2009 *Adv. Mater.* **21** 2463
[47] Liu Y, Wang Y, Ma J, Li S, Pan H, Nan C W and Lin Y H 2022 *Prog. Mater. Sci.* **127** 100943
[48] Zak A K and Hashim A M 2025 *Coord. Chem. Rev.* **523** 216297
[49] Lorenz B 2013 *ISRN Condens. Matter Phys.* **2013** 497073
[50] Tomuta D G, Ramakrishnan S, Nieuwenhuys G J and Mydosh J A 2001 *J. Phys.: Condens. Matter* **13** 4543
[51] Katsufuji T, Masaki M, Machida A, Moritomo M, Kato K, Nishibori E, Takata M, Sakata M, Ohoyama K, Kitazawa K and Takagi H 2002 *Phys. Rev. B* **66** 134434
[52] Yen F, Dela Cruz C, Lorenz B, Galstyan E, Sun Y Y, Gospodinov M and Chu C W 2007 *J. Mater. Res.* **22** 2163
[53] Park S, Choi Y J, Zhang C L and Cheong S W 2007 *Phys. Rev. Lett.* **98** 057601
[54] Zhang J J, Lin L, Zhang Y, Wu M, Yakobson B I and Dong S 2018 *J. Am. Chem. Soc.* **140** 9768
[55] Sødequist J and Olsen T 2023 *2D Mater.* **10** 035016
[56] Lu C and Liu J M 2016 *J. Materiomics* **2** 213
[57] Zhu W, Wang P, Zhu H, Zhu H, Li X, Zhao J, Xu C and Xiang H 2025 *Phys. Rev. Lett.* **134** 066801
[58] Patureau P, Dessapt R, Deniard P, Chung U C, Michau D, Josse M, Payen C and Maglione M 2016 *Chem. Mater.* **28** 7582
[59] Dzyaloshinsky I 1958 *J. Phys. Chem. Solids* **4** 241
[60] Moriya T 1960 *Phys. Rev.* **120** 91
[61] Katsura H, Nagaosa N and Balatsky A V 2005 *Phys. Rev. Lett.* **95** 057205
[62] Fumega A O and Lado J L 2022 *2D Mater.* **9** 025010
[63] Ju H, Lee Y, Kim K T, Choi I H, Roh C J, Son S, Park P, Kim J H, Jung T S, Kim J H, Kim K H, Park J G and Lee J S 2021 *Nano Lett.* **21** 5126
[64] Song Q, Occhialini C A, Ergeçen E, Ilyas B, Amoroso D, Barone P, Kapeghian J, Watanabe K, Taniguchi T, Botana A S, Picozzi S, Gedik N and Comin R 2022 *Nature* **602** 601
[65] Chu H, Roh C J, Island J O, Li C, Lee S, Chen J, Joung S L and Hsieh D 2020 *Phys. Rev. Lett.* **124** 027601
[66] Park C B, Shahee A, Kim K T, Patil D R, Guda S A, Ter-Oganessian N and Kim K H 2022 *Adv. Electron. Mater.* **8** 2101072
[67] Vaz C A F and Staub U 2013 *J. Mater. Chem. C* **1** 6731
[68] Taniyama T, Gohda Y, Hamaya K and Kimura T 2024 *Sci. Technol. Adv. Mater.* **25** 2412970
[69] Zhao X, Feng M, Liu M, Hua J, Ma J, Wu L, Xu H, Wang A and Li H B 2018 *Mater. Res. Lett.* **6** 592
[70] Pan L, Pan M, Hu J, Hu Y, Che Y, Yu Y, Wang N, Qiu W, Li P, Peng J and Jiang J 2020 *Sensors* **20** 1440
[71] Heron J T, Bosse J L, He Q, Gao Y, Trassin M, Ye L, Clarkson J D, Wang C, Liu J, Salahuddin S, Ralph D C, Schlom D G, Iniguez J, Huey B D and Ramesh R 2014 *Nature* **516** 370
[72] Chappert C, Fert A and Van Dau F N 2007 *Nat. Mater.* **6** 813
[73] Allwood D A, Xiong G, Faulkner C C, Atkinson D, Petit D and Cowburn R P 2005 *Science* **309** 1688
[74] Venkataiah G, Shirahata Y, Itoh M and Taniyama T 2011 *Appl. Phys. Lett.* **99** 102506
[75] Sahoo S, Polisetty S, Duan C G, Jaswal S S, Tsymbal E Y and Binek C 2007 *Phys. Rev. B* **76** 092108
[76] Hirohata A and Takanashi K 2014 *J. Phys. D: Appl. Phys.* **47** 193001
[77] Cai T, Ju S, Lee J, Sai N, Demkov A A, Niu Q, Li Z, Shi J and Wang E 2009 *Phys. Rev. B* **80** 140415
[78] Lahtinen T H E, Franke K J A and van Dijken S 2012 *Sci. Rep.* **2** 258
[79] Chu Y H, Martin L W, Holcomb M B, Gajek M, Han S J, He Q, Balke N, Yang C H, Lee D, Hu W, Zhan Q, Yang P L, Fraile-Rodriguez A, Scholl A, Wang S X and Ramesh R 2008 *Nat. Mater.* **7** 478
[80] Pesquera D, Khestanova E, Ghidini M, Zhang S, Rooney A P, Maccherozzi F, Riego P, Farokhiipoor S, Kim J, Moya X, Vickers M E, Stelmashenko N A, Haigh S J, Dhesi S S and Mathur N D 2020 *Nat. Commun.* **11** 3190
[81] Thiele C, Dörr K, Bilani O, Rödel J and Schultz L 2007 *Phys. Rev. B* **75** 054408
[82] Bréhin J, Chen Y, D'Antuono M, Varotto S, Stornaiuolo D, Piamonteze C, Varignon J, Salluzzo M and Bibes M 2023 *Nat. Phys.* **19** 823
[83] Geim A K and Grigorieva I V 2013 *Nature* **499** 419
[84] Liu Y, Weiss N O, Duan X, Cheng H C, Huang Y and Duan X 2016 *Nat. Rev. Mater.* **1** 1
[85] Novoselov K S, Mishchenko A, Carvalho A and Castro Neto A H 2016 *Science* **353** aac9439
[86] Jariwala D, Marks T J and Hersam M C 2017 *Nat. Mater.* **16** 170
[87] Castellanos-Gomez A, Duan X, Fei Z, Gutierrez H R, Huang Y, Huang X, Quereda J, Qian Q, Sutter E and Sutter P 2022 *Nat. Rev. Methods Primers* **2** 58
[88] Jiang S, Shan J and Mak K F 2018 *Nat. Mater.* **17** 406
[89] Jiang P, Wang C, Chen D, Zhong Z, Yuan Z, Lu Z Y and Ji W 2019 *Phys. Rev. B* **99** 144401
[90] Deiseroth H J, Aleksandrov K, Reiner C, Kienle L and Kremer R K 2006 *Eur. J. Inorg. Chem.* **2006** 1561
[91] Deng Y, Yu Y, Song Y, Zhang J, Wang N Z, Sun Z, Yi Y, Wu Y Z, Wu S, Zhu J, Wang J, Chen X H and Zhang Y 2018 *Nature* **563** 94
[92] Gong C, Kim E M, Wang Y, Lee G and Zhang X 2019 *Nat. Commun.* **10** 2657
[93] Wu Y, Zhang D, Zhang Y N, Deng L and Peng B 2024 *Nano Lett.* **24** 5929
[94] Sarmah H S and Ghosh S 2025 *J. Phys. Chem. C* **129** 6466
[95] Li Z and Zhou B 2020 *J. Mater. Chem. C* **8** 4534
[96] Hunt B, Sanchez-Yamagishi J D, Young A F, Yankowitz M, LeRoy B J, Watanabe K, Taniguchi T, Moon P, Jarillo-Herrero P and Ashoori R C 2013 *Science* **340** 1427
[97] Dean C R, Wang L, Maher P, Forsythe C, Ghahari F, Gao Y, Katoch J, Ishigami M, Moon P, Koshino M, Taniguchi T, Watanabe K, Sheparde K L, Hone J and Kim P 2013 *Nature* **49** 598
[98] Tong Q, Yu H, Zhu Q, Wang Y, Xu X and Yao W 2017 *Nat. Phys.* **13** 356
[99] Li Y, Wan Q and Xu N 2025 *Adv. Mater.* **37** 2305175
[100] Muneeswaran M, Gopiraman M, Dhanabalan S S, Giridharan N V and Akbari-Fakhrabadi A 2021 *Metal and Metal Oxides for Energy and Electronics* edn Rajendran S, Qin J, Gracia F and Lichtfouse E (Cham: Springer International Publishing) pp. 375–395
[101] Ahmad T, Jindal K, Tomar M and Jha P K 2023 *Mater. Today Commun.* **37** 107516
[102] Spaldin N A and Ramesh R 2019 *Nat. Mater.* **18** 203
[103] Arya G S and Negi N S 2013 *J. Phys. D: Appl. Phys.* **46** 095004
[104] Awasthi R R and Das B 2019 *Optik* **194** 162973
[105] Golda R A, Marikani A and Alex E J 2020 *Ceram. Int.* **46** 1962
[106] Sharma S, Kumar A, Thakur O P and Saharan P 2024 *J. Electron. Mater.* **53** 6110
[107] Hu Y C, Jiang Z Z, Gao K G, Cheng G F, Ge J J, Lv X M and Wu X S 2012 *Chem. Phys. Lett.* **534** 62
[108] Zhao Y, Zhang J J, Yuan S and Chen Z 2019 *Adv. Funct. Mater.* **29** 1901420
[109] Lu Y, Fei R, Lu X, Zhu L, Wang L and Yang L 2020 *ACS Appl. Mater. Interfaces* **12** 6243
[110] Eerenstein W, Mathur N D and Scott J F 2006 *Nature* **442** 759
[111] Zhang K, Wang X and Mi W 2023 *Phys. Chem. Chem. Phys.* **25** 19773
[112] Gamow G 1928 *Z. Angew. Phys.* **51** 204
[113] Frenkel J 1930 *Phys. Rev.* **36** 1604
[114] Esaki L 1958 *Phys. Rev.* **109** 603
[115] Giaever I 1960 *Phys. Rev. Lett.* **5** 464
[116] Josephson B D 1962 *Phys. Lett.* **1** 251
[117] Gregg J F, Petej I, Jouguelet E and Dennis C 2002 *J. Phys. D: Appl. Phys.* **35** R121
[118] Moodera J S, Kinder L R, Wong T M and Meservey R 1995 *Phys. Rev. Lett.* **74** 3273
[119] Parkin S S, Kaiser C, Panchula A, Rice P M, Hughes B, Samant M and Yang S H 2004 *Nat. Mater.* **3** 862
[120] Garcia V and Bibes M 2014 *Nat. Commun.* **5** 4289
[121] Tsymbal E Y and Kohlstedt H 2006 *Science* **313** 181
[122] Luo K F, Ma Z, Sando D, Zhang Q and Valanoor N 2025 *ACS Nano* **19** 6622
[123] Zhang X, Zhou Z, Yu X, Guo Y, Chen Y and Wang J 2023 *Adv. Funct. Mater.* **33** 2301353

[124] Watanabe K, Jinnai B, Fukami S, Sato H and Ohno H 2018 *Nat. Commun.* **9** 663
[125] Yan Z, Xiao J, Zhang X, Fang C and Xu X 2026 *Adv. Funct. Mater.* **36** e11719
[126] Julliere M 1975 *Phys. Lett. A* **54** 225
[127] Song T, Cai X, Tu M W Y, Zhang X, Huang B, Wilson N P, Seyler K, Zhu L, Taniguchi T, Watanabe K, McGuire M A, Cobden D H, Xiao D, Yao W and Xu X 2018 *Science* **360** 1214
[128] Yuasa S and Djayaprawira D D 2007 *J. Phys. D: Appl. Phys.* **40** R337
[129] Miyazaki T and Tezuka N 1995 *J. Magn. Magn. Mater.* **139** L231
[130] Butler W H, Zhang X G, Schulthess T C and MacLaren J M 2001 *Phys. Rev. B* **63** 054416
[131] Mathon J and Umerski A 2001 *Phys. Rev. B* **63** 220403
[132] Ikeda S, Hayakawa J, Ashizawa Y, Lee Y M, Miura K, Hasegawa H, Tsunoda M, Matsukura F and Ohno H 2008 *Appl. Phys. Lett.* **93** 082508
[133] Scheike T, Wen Z, Sukegawa H and Mitani S 2023 *Appl. Phys. Lett.* **122** 112404
[134] Yan Z, Zhang R, Dong X, Qi S and Xu X 2020 *Phys. Chem. Chem. Phys.* **22** 14773
[135] Huang B, Clark G, Navarro-Moratalla E, Klein D R, Cheng R, Seyler K L, Zhong D, Schmidgall E, McGuire M A, Cobden D H, Yao W, Xiao D, Jarillo-Herrero P and Xu X 2017 *Nature* **546** 270
[136] Yuasa S, Nagahama T and Suzuki Y 2002 *Science* **297** 234
[137] Liu J, Sun Q, Kawazoe Y and Jena P 2016 *Phys. Chem. Chem. Phys.* **18** 8777
[138] Li X, Lu J T, Zhang J, You L, Su Y and Tsymbal E Y 2019 *Nano Lett.* **19** 5133
[139] Wang Z, Sapkota D, Taniguchi T, Watanabe K, Mandrus D and Morpurgo A F 2018 *Nano Lett.* **18** 4303
[140] An Z, Su Y, Ni S and Guan Z 2022 *J. Phys. Chem. C* **126** 11330
[141] Kohlstedt H, Pertsev N A, Rodríguez Contreras J and Waser R 2005 *Phys. Rev. B* **72** 125341
[142] Zhuravlev M Y, Sabirianov R F, Jaswal S S and Tsymbal E Y 2005 *Phys. Rev. Lett.* **94** 246802
[143] Ma Z, Zhang Q and Valanoor N 2020 *Appl. Phys. Rev.* **7** 041316
[144] Wen Z and Wu D 2020 *Adv. Mater.* **32** 1904123
[145] Borisov V S, Ostanin S, Achilles S, Henk J and Mertig I 2015 *Phys. Rev. B* **92** 075137
[146] Garcia V, Bibes M, Bocher L, Valencia S, Kronast F, Crassous A, Moya X, Enouz-Vedrenne S, Gloter A, Imhoff D, Deranlot C, Mathur N D, Fusil S, Bouzehouane K and Barthélémy A 2010 *Science* **327** 1106
[147] Wan S, Li Y, Li W, Mao X, Zhu W and Zeng H 2018 *Nanoscale* **10** 14885
[148] Li L 2016 *J. Phys. Chem. C* **120** 24857
[149] Lakshmy S, Mondal B, Kalarikkal N, Rout C S and Chakraborty B 2024 *Adv. Powder Mater.* **3** 100204
[150] Tsymbal E Y, Gruverman A, Garcia V, Bibes M and Barthélémy A 2012 *MRS Bull.* **37** 138
[151] Zhang L, Wang Y, Liu X and Liu F 2022 *npj Comput. Mater.* **8** 197
[152] Zhu Y, Chi B, Jiang L, Guo X, Yan Y and Han X 2023 *Phys. Rev. Appl.* **20** 034010
[153] Duan C G, Jaswal S S and Tsymbal E Y 2006 *Phys. Rev. Lett.* **97** 047201
[154] Cao D, Cai M Q, Hu W Y and Xu C M 2011 *J. Appl. Phys.* **109** 114107
[155] Velev J P, Duan C G, Burton J D, Smogunov A, Niranjan M K, Tosatti E, Jaswal S S and Tsymbal E Y 2009 *Nano Lett.* **9** 427
[156] Gajek M, Bibes M, Fusil S, Bouzehouane K, Fontcuberta J, Barthélémy A and Fert A 2007 *Nat. Mater.* **6** 296
[157] Su Y, Li X, Zhu M, Zhang J, You L and Tsymbal E Y 2020 *Nano Lett.* **21** 175
[158] Bai H, Li X, Pan H, He P, Xu Z A and Lu Y 2021 *ACS Appl. Mater. Interfaces* **13** 60200
[159] Yan Z, Li Z, Han Y, Qiao Z and Xu X 2022 *Phys. Rev. B* **105** 075423
[160] Yu C, Li X, Li X and Yang J 2021 *J. Phys. Chem. Lett.* **12** 11790
[161] Cui Z, Sa B, Xue K H, Zhang Y, Xiong R, Wen C, Miao X and Sun Z 2024 *Nanoscale* **16** 1331
[162] Guo X H, Zhu L, Cao Z L and Yao K L 2024 *Phys. Chem. Chem. Phys.* **26** 3531
[163] Li L and Wu M 2017 *ACS Nano* **11** 6382
[164] Wu M 2021 *ACS Nano* **15** 9229
[165] Vizner Stern M, Waschitz Y, Cao W, Nevo I, Watanabe K, Taniguchi T, Sela E, Urbakh M, Hod O and Ben Shalom M 2021 *Science* **372** 1462
[166] Dong X, Shen X, Sun X, Bai Y, Yan Z and Xu X 2023 *Phys. Rev. B* **108** 085427
[167] Yan Z, Yang R, Fang C, Lu W and Xu X 2024 *Phys. Rev. B* **109** 205409
[168] Feng Y, Han J, Zhang K, Lin X, Gao G, Yang Q and Meng S 2024 *Phys. Rev. B* **109** 085433
[169] Yang R, Zhang X, Xiao J, Yan Z, Wang F and Xu X 2025 *Chin. Phys. Lett.* **42** 070705
[170] Yu X, Zhang X and Wang J 2023 *ACS Nano* **17** 25348
[171] Yan Z, Zhang X, Xiao J, Fang C and Xu X 2025 *Nano Lett.* **25** 8473
[172] Dal Din A, Amin O J, Wadley P and Edmonds K W 2024 *npj Spintronics* **2** 25
[173] Han J, Cheng R, Liu L, Ohno H and Fukami S 2023 *Nat. Mater.* **22** 684
[174] Qin P, Yan H, Wang X, Chen H, Meng Z, Dong J, Zhu M, Cai J, Feng Z, Zhou X, Liu L, Zhang T, Zeng Z, Zhang Z, Zhang J, Jiang C and Liu Z 2023 *Nature* **613** 485
[175] Gu P, Wang C, Su D, Dong Z, Wang Q, Han Z, Watanabe K, Taniguchi T, Sun Y and Ye Y 2023 *Nat. Commun.* **14** 3221
[176] Yan Z, Qiao D, Lu W, Dong X and Xu X 2025 *Phys. Rev. B* **111** 045404
[177] Sun Z, Su Y, Zhi A, Gao Z, Han X, Wu K, Bao L, Huang Y, Shi Y, Bai X, Cheng P, Chen L, Wu K, Tian X, Wu C and Feng B 2024 *Nat. Commun.* **15** 4252
[178] He K, Liu X, Yu G, Zhang Y, Zhang Y, Zhu S and Shen L 2025 *ACS Appl. Nano Mater.* **8** 9145
[179] Jungwirth T, Sinova J, Manchon A, Marti X, Wunderlich J and Felser C 2018 *Nat. Phys.* **14** 200
[180] Jungwirth T, Marti X, Wadley P and Wunderlich J 2016 *Nat. Nanotechnol.* **11** 231
[181] Yuan L D, Wang Z, Luo J W and Zunger A 2021 *Phys. Rev. Mater.* **5** 014409
[182] Gurung G, Shao D F and Tsymbal E Y 2021 *Phys. Rev. Mater.* **5** 124411
[183] Yang H, Sun Y, Zhang Y, Shi W J, Parkin S S and Yan B 2017 *New J. Phys.* **19** 015008
[184] Yu T, Liu R, Peng Y, Zheng P, Wang G, Ma X, Yuan Z and Yin Z 2022 *Phys. Rev. B* **10** 205103
[185] Železný J, Zhang Y, Felser C and Yan B 2017 *Phys. Rev. Lett.* **119** 187204
[186] Zhang Y, Sun Y, Yang H, Železný J, Parkin S P, Felser C and Yan B 2017 *Phys. Rev. B* **95** 075128
[187] Zhang X, Yin L, Zhu S, Cheng R, Wen Y and He J 2022 *Phys. Rev. B* **110** 024428
[188] Dong J, Li X, Gurung G, Zhu M, Zhan P, Zheng F, Tsymbal E Y and Zhang J 2022 *Phys. Rev. Lett.* **128** 197201
[189] Soh J R, De Juan F, Qureshi N, Jacobsen H, Wang H Y, Guo Y F and Boothroyd A T 2020 *Phys. Rev. B* **101** 140411
[190] Han R K, Zhao X P, Qin H R, Sun H L, Wang H L, Wei D H and Zhao J H 2023 *Phys. Rev. B* **107** 134422
[191] Bai H, Zhou X F, Zhang H W, Kong W W, Liao L Y, Feng X Y, Chen X Z, You Y F, Han L, Zhu W X, Pan F, Fan X L and Song C 2021 *Phys. Rev. B* **104** 104401
[192] Guo L, Campbell N, Grutter A J, Noh G, Nan T, Quarterman P, Choi S Y, Tybell T, Rzchowski M S and Eom C B 2024 *Phys. Rev. Mater.* **8** L011401
[193] Šmejkal L, Sinova J and Jungwirth T 2022 *Phys. Rev. X* **12** 031042
[194] Šmejkal L, Sinova J and Jungwirth T 2022 *Phys. Rev. X* **12** 040501
[195] González-Hernández R, Šmejkal L, Výborný K, Yahagi Y, Sinova J, Jungwirth T and Železny J 2021 *Phys. Rev. Lett.* **126** 127701
[196] Šmejkal L, Hellenes A B, González-Hernández R, Sinova J and Jungwirth T 2022 *Phys. Rev. X* **12** 011028
[197] Karube S, Tanaka T, Sugawara D, Kadoguchi N, Kohda M and Nitta J 2022 *Phys. Rev. Lett.* **129** 137201
[198] Yang G, Li Z, Yang S, Li J, Zheng H, Zhu W, Pan Z, Xu Y, Cao S, Zhao W, Jana A, Zhang J, Ye M, Song Y, Hu L H, Yang L, Jun F, Vobornik I, Shi M, Yuan H, Zhang Y, Xu Y and Liu Y 2025 *Nat. Commun.* **16** 1442
[199] Liu Z, Ozeki M, Asai S, Itoh S and Masuda T 2024 *Phys. Rev. Lett.* **133** 156702
[200] Yuan L D, Wang Z, Luo J W, Rashba E I and Zunger A 2020 *Phys. Rev. B* **102** 014422
[201] Cui Q, Zhu Y, Yao X, Cui P and Yang H 2023 *Phys. Rev. B* **108** 024410
[202] Zhang L, Ni G, He J and Gao G 2025 *Phys. Rev. B* **112** 064401
[203] Wang S X, Qiao S X, Ni M Y, Zheng X H, Hao H, Lu H Y and Zhang P 2025 *Chin. Phys. Lett.* **42** 080701

[204] Yang S, Liu C S, Yu S, Jiang P, Hao H, Zhang L, Liu S and Zheng X 2025 *Chin. Phys. Lett.* **42** 090705
[205] Zhang J J, Lin L, Zhang Y, Wu M, Yakobson B I and Dong S 2018 *J. Am. Chem. Soc.* **140** 9768
[206] Liu X, Pyatakov A P and Ren W 2020 *Phys. Rev. Lett.* **125** 247601
[207] Gu P, Wang C, Su D, Dong Z, Wang Q, Han Z, Watanabe K, Taniguchi T, Ji W, Sun J and Ye Y 2023 *Nat. Commun.* **14** 3221
[208] Liang S, Xie T, Blumenschein N A, Zhou T, Ersevim T, Song Z, Liang J, Susner M A, Conner B S, Gong S, Wang J, Ouyang M, Zutic I, Friedman A L, Zhang X and Gong C 2023 *Nat. Electron.* **6** 199
[209] Eom J, Lee I H, Kee J Y, Cho M, Seo J, Suh H, Choi H, Sim Y, Chen S, Chang H J, Baek S, Petromir C, Ryu H, Jang C, Kim Y D, Yang C, Seong M, Lee J H, Park S Y and Choi J W 2023 *Nat. Commun.* **14** 5605
[210] Wu Y, Zhang D, Zhang Y N, Deng L and Peng B 2024 *Nano Lett.* **24** 5929
[211] Wang Q, Yan J, Gao X, Yu Z, Yue D, Mu C, Cheng Y, Nie A, Xue T, Liu L and Zhai K 2025 *Small* **21** e10429
[212] Zhao H, Yang C, Liu Y, Wang Q, Wu Y, Mu Q, Hou F, Min T and Li T 2025 *Adv. Mater.* **37** 2500534
[213] Zhao Y, Bao C, Zhan Y, Du K, Huang W and Su C 2022 *Mater. Lett.* **324** 132687
[214] Zhou T, Zhai T, Shen H, Wang J, Min R, Ma K and Zhang G 2023 *Chemosphere* **339** 139678
[215] Gibertini M, Koperski M, Morpurgo A F and Novoselov K S 2019 *Nat. Nanotechnol.* **14** 408
[216] Gong C and Zhang X 2019 *Science* **363** eaav4450
[217] Yi M and Shen Z 2015 *J. Mater. Chem. A* **3** 11700
[218] Shen P C, Lin Y, Wang H, Park J H, Leong W S and Lu A Y 2018 *IEEE Trans. Electron Devices* **65** 4040
[219] Samad L, Bladow S M, Ding Q, Zhuo J, Jacobberger R M, Arnold M S and Jin S 2016 *ACS Nano* **10** 7039
[220] Hossain M, Qin B, Li B and Duan X 2022 *Nano Today* **42** 101338